Computer Aided Geometric Design 47 (2016) 61–82

Contents lists available at ScienceDirect

Computer Aided Geometric Design

www.elsevier.com/locate/cagd

Unstructured spline spaces for isogeometric analysis based on spline manifolds

Giancarlo Sangalli [a,b], Thomas Takacs [a,*], Rafael Vázquez [b]

[a] Dipartimento di Matematica "F. Casorati", Università degli Studi di Pavia, Italy
[b] Istituto di Matematica Applicata e Tecnologie Informatiche "E. Magenes" (CNR), Italy

ARTICLE INFO

Article history:
Available online 27 May 2016

Keywords:
Spline manifold
Isogeometric analysis
Unstructured T-splines
Multi-patch

ABSTRACT

Based on Grimm and Hughes (1995) we introduce and study a mathematical framework for analysis-suitable unstructured B-spline spaces. In this setting the parameter domain has a manifold structure which allows for the definition of function spaces such as, for instance, B-splines over multi-patch domains with extraordinary points or analysis-suitable unstructured T-splines. Within this framework, we generalize the concept of dual-compatible B-splines (developed for structured T-splines in Beirão da Veiga et al. (2013)). This allows us to prove the key properties that are needed for isogeometric analysis, such as linear independence and optimal approximation properties for h-refined meshes.

1. Introduction

Isogeometric analysis (IgA), as it was introduced in Hughes et al. (2005), is a discretization method that directly uses the geometry models as they are present in CAD for the numerical solution of partial differential equations, without the need of generating a mesh. In the basic setting of IgA the physical domain of interest is parametrized by tensor-product B-splines or NURBS, therefore it has to be diffeomorphic to a rectangle or hexahedron. In a broader context, the discretization is based on the geometry representation as it is implemented in the CAD system. Hence, there is a need for a more flexible geometry representation beyond tensor-product splines. Within the CAD community there exist several approaches to enhance the geometric flexibility, such as multi-patch representations, unstructured T-splines or subdivision methods, among others. These approaches have been also applied in IgA, with the same objective of obtaining more flexible representations of the physical domain.

The first attempts to introduce more complicated geometric models in IgA were focused on multi-patch representations, already addressed in Cottrell et al. (2009), and developed in several recent contributions (Kiendl et al., 2010; Beirão da Veiga et al., 2011; Kleiss et al., 2012; Xu et al., 2013; Jüttler et al., 2014; Scott et al., 2014; Buchegger et al., 2015). The idea is to define the domain as the image of several rectangles (or hexahedra), called patches, that have to be glued together at the interfaces. In most constructions the basis functions are only C^0 across patch interfaces, but we want to point out the recent paper (Buchegger et al., 2015), in which the smoothness across patch interfaces is enhanced away from extraordinary features by increasing the parametric continuity. Another approach to realize higher order smoothness on multi-patch geometries is via geometric continuity, see for instance (Nguyen et al., 2014b, 2016; Groisser and Peters, 2015; Kapl et al., 2015a, 2015b; Collin et al., 2015). In all those configurations the starting point is a C^0 multi-patch configuration. To increase the smoothness across patch interfaces, additional geometric continuity conditions are imposed.

* Corresponding author.
E-mail address: thomas.takacs@jku.at (T. Takacs).

http://dx.doi.org/10.1016/j.cagd.2016.05.004
0167-8396/

Another way to handle complex geometries is to use a specific space of non-tensor product functions, such as unstructured T-splines (Sederberg et al., 2003). In this case, the T-spline functions are defined via their contributions within the (quadrilateral or hexahedral) elements of a T-mesh, and the underlying elemental T-mesh has a manifold structure. The construction of unstructured T-splines for their use in IgA has been studied in Wang et al. (2011, 2012), reducing the continuity of the spline functions in the vicinity of extraordinary features, as well as in Scott et al. (2013), in this case raising the degree in the elements adjacent to extraordinary points.

Smooth constructions over general meshes can also be introduced by means of subdivision surfaces. They have been studied in the context of IgA in, e.g., Barendrecht et al. (2013), Burkhart et al. (2010), Cirak and Ortiz (2001), Cirak et al. (2000), Nguyen et al. (2014b), Jüttler et al. (2015). While subdivision constructions are based on a manifold, they do not fit into our specific spline manifold framework, since we require the functions to be piecewise polynomials on a given mesh. Indeed, function spaces based on classical subdivision schemes (e.g., Doo-Sabin (1978) for biquadratics or Catmull-Clark (1978) for bicubics) are spanned by B-splines but also by special geometrically continuous functions near extraordinary points. These special functions are piecewise polynomials over infinitely many rings of quadrilateral elements.

Despite their differences, all these approaches have in common an underlying manifold structure which allows to handle complex geometries with extraordinary points or edges. In this work we propose the use of spline manifold spaces to introduce a common general framework that is valid for the definition and the study of these different approaches. We note that it is not the purpose of this paper to introduce a new way to define or implement unstructured spline spaces. The aim is rather to develop a framework for studying the theoretical properties of a wide range of spline representations over non-rectangular parameter domains based on manifolds. Within this framework we focus on the formal definition of a basis, a corresponding dual basis and an L^2-stable spline projector. This projector is then used to prove approximation error bounds on a spline manifold domain. It is worth to remark that an exhaustive, uniform mathematical theory for all the approaches mentioned above is still missing. We would also like to point out that we do not address the problem of trimming here, even though it is a standard procedure in CAD. The concept of trimming extends the flexibility of the geometry representation and it can be generalized straight-forwardly to spline manifolds.

The idea of spline manifolds was first developed in Grimm and Hughes (1995), where the authors present a constructive approach to build a manifold from a polyhedral "sketch" using splines. Despite the constructive approach in the paper, the method relies on an abstraction of the concept of geometry parametrization, that includes parameter domains with a manifold structure. This structure is then inherited by the constructed physical domain. Our framework for the analysis of unstructured spline spaces makes use of this abstraction, that we briefly review now.

We consider a domain $\Sigma \subset \mathbb{R}^n$ which can be interpreted as a d-dimensional manifold with $d \leq n$, but we mostly focus on planar surfaces ($d = n = 2$), three-dimensional surfaces ($d = 2, n = 3$) and volumetric domains ($d = n = 3$). In an abstract setting, the manifold Σ is defined by an *atlas*, i.e., a family of *charts* Σ_i such that they cover completely the domain

$$\Sigma = \bigcup_{i=1}^{N} \Sigma_i,$$

together with a collection of suitable *transition maps* between intersecting charts Σ_i and Σ_j. In the setting introduced in Grimm and Hughes (1995), one first defines a family of *open* parameter subdomains Ω_i, along with a spline space on each subdomain. Then each chart is the image of a *spline parametrization* $\mathbf{G}_i : \Omega_i \to \Sigma_i$. The union of the subdomains Ω_i forms an unstructured parameter domain Ω, and suitable transition functions between the parametric subdomains endow Ω with a manifold structure. Introducing a relation between the spline spaces on the subdomains, this manifold structure is then inherited by the physical domain Σ.

Notice that to cover completely the domain Σ, the charts Σ_i, and also the open parameter subdomains Ω_i must overlap. Hence, in order to cover the extraordinary points (or edges) it is necessary that some of the subdomains Ω_i also have an unstructured configuration, and non-tensor product spline functions need to be defined. This is in contrast to traditional multi-patch representations, where only the patch boundaries intersect, and the (closed) domain is defined as the union of the closure of the patches.

Although the framework of spline manifolds can be used to define and study the constructions mentioned above, namely, multi-patch configurations and unstructured T-splines, it is out of the scope of this paper to analyze each of them. Instead, we will apply the framework to generalize the concept of dual-compatible T-splines, introduced in Beirão da Veiga et al. (2012a, 2013) for structured T-splines, to unstructured T-splines with low continuity in the neighborhood of the extraordinary points. With the dual-compatibility condition it is possible to define a dual basis, which is then used to prove that these spaces have the key properties that are needed for their use in IgA, such as linear independence of the basis functions, and optimal approximation properties under h-refinement.

The remainder of the paper is organized as follows. In Section 2 we recall in detail the notion of a parameter manifold as presented in Grimm and Hughes (1995). We introduce the mesh on the parameter manifold and corresponding mesh constraints in Section 3. In Section 4 we introduce spline manifold spaces based on tensor product B-splines and relate them to existing constructions (Buchegger et al., 2015; Wang et al., 2011, 2012; Scott et al., 2013). Finally, we develop the framework of analysis suitable spline manifold spaces in Section 5, where we extend the notion of dual-compatibility to

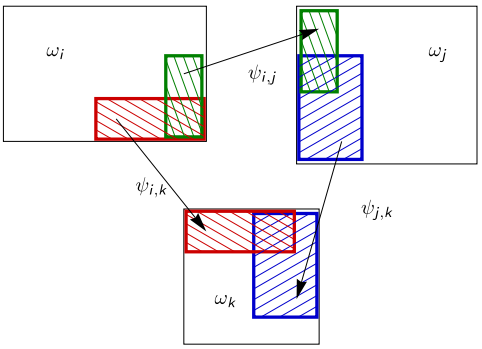

Fig. 1. Visualization of the cocycle condition.

B-spline manifolds. In the main part of the paper we assume that the manifold has no boundary. For a more detailed study of spline manifolds with boundary see Appendix A. We conclude the paper and present possible extensions in Section 6.

2. Parameter manifold

Before we can define unstructured spline spaces on manifolds we need to introduce the abstract representation of the parameter domain, the so-called *parameter manifold*. The following definitions are taken from Grimm and Hughes (1995). The definitions are valid for arbitrary dimension d, but we will mostly consider $d = 1, 2, 3$.

Definition 1 *(Proto-manifold).* A proto-manifold of dimension d consists of

- a finite set $\{\omega_i\}_{i=1,\dots,N}$ (named *proto-atlas*) of *charts* ω_i, that are open polytopes $\omega_i \subset \mathbb{R}^d$, line segments for $d = 1$, polygons for $d = 2$ or polyhedra for $d = 3$;
- a set of open *transition domains* $\{\omega_{i,j}\}_{i,j=1,\dots,N}$ that are polytopes such that $\omega_{i,j} \subset \omega_i$, $\omega_{i,i} = \omega_i$, and each $\omega_{i,j}$ is the interior of its closure;
- a set of *transition functions* $\{\psi_{i,j}\}_{i,j=1,\dots,N}$, that are homeomorphisms $\psi_{i,j} : \omega_{i,j} \to \omega_{j,i}$ fulfilling the *cocycle condition* $\psi_{j,k} \circ \psi_{i,j} = \psi_{i,k}$ in $\omega_{i,j} \cap \omega_{i,k}$ for all $i, j, k = 1, \dots, N$;
- For every i, j, with $i \neq j$, for every $\boldsymbol{\zeta}_i \in \partial\omega_{i,j} \cap \omega_i$ and $\boldsymbol{\zeta}_j \in \partial\omega_{j,i} \cap \omega_j$, there are open balls, $V_{\boldsymbol{\zeta}_i}$ and $V_{\boldsymbol{\zeta}_j}$, centered at $\boldsymbol{\zeta}_i$ and $\boldsymbol{\zeta}_j$, such that no point of $V_{\boldsymbol{\zeta}_j} \cap \omega_{j,i}$ is the image of any point of $V_{\boldsymbol{\zeta}_i} \cap \omega_{i,j}$ by $\psi_{j,i}$.

In Fig. 1 we visualize the cocycle condition, depicting three domains ω_i, ω_j and ω_k and respective transition functions $\psi_{i,j}$, $\psi_{j,k}$ and $\psi_{i,k}$. The hatched regions represent corresponding transition domains.

The transition domains $\omega_{i,j}$ may be empty. It follows directly from the cocycle condition that the transition function $\psi_{i,i}$ is the identity function on $\omega_{i,i} = \omega_i$ and that $\psi_{i,j}^{-1} = \psi_{j,i}$ for all i, j.

Remark 1. The last condition in Definition 1 is taken from Siqueira et al. (2009). It guarantees that the proto-manifold actually represents a manifold, i.e. that there are no bifurcations of the domain. Note that this condition is not necessary for the following definitions. However, if the condition is omitted, the resulting object is not a manifold anymore.

By merging and identifying the charts of the proto-manifold we obtain a manifold, which will serve as the parameter domain in our setting, thus the name *parameter manifold*.

Definition 2 *(Parameter manifold).* Given a proto-manifold, the set

$$\Omega = \left(\bigsqcup_{i=1,\dots,N} \omega_i \right) \Big/ \sim \tag{1}$$

is called a *parameter manifold*. Here $\bigsqcup$ denotes the disjoint union, i.e.,

$$\bigsqcup_{i=1,\dots,N} \omega_i = \left\{ [\boldsymbol{\zeta}_i, i],\ \boldsymbol{\zeta}_i \in \omega_i, i = 1, \dots, N \right\}$$

and the equivalence relation $\sim$ is defined for all $\boldsymbol{\zeta}_i \in \omega_i$ and $\boldsymbol{\zeta}_j \in \omega_j$, as

$$[\boldsymbol{\zeta}_i, i] \sim [\boldsymbol{\zeta}_j, j] \Leftrightarrow \psi_{i,j}(\boldsymbol{\zeta}_i) = \boldsymbol{\zeta}_j.$$

We denote by $\pi_i(\boldsymbol{\zeta}_i) \in \Omega$ the equivalence class corresponding to $\boldsymbol{\zeta}_i \in \omega_i$.

In the following we use the notation $\Omega_i = \pi_i(\omega_i)$ and $\Omega_{i,j} = \pi_i(\omega_{i,j})$, where $\Omega_i, \Omega_{i,j} \subset \Omega$. Hence we have $\Omega_{i,j} = \Omega_{j,i} = \Omega_i \cap \Omega_j$. Note that π_i is a one-to-one correspondence between each ω_i and Ω_i, and plays the role of a local representation.

To motivate the definition (and wording) above, we recall the following result, which states that Ω is indeed a manifold (see Grimm and Hughes, 1995; Siqueira et al., 2009).

Proposition 1. *Given a proto-manifold, the set Ω as in Definition 2 is a topological manifold, where the inverse π_i^{-1} of the mapping π_i is the coordinate chart corresponding to the set $\Omega_i \subset \Omega$.*

To be more precise, a parameter manifold is a class of piecewise smooth manifolds, which is a sub-class of topological manifolds and a super-class of smooth manifolds. It is similar to the concept of piecewise linear manifolds (see Rourke and Sanderson, 1972). Depending on its local structure, the parameter manifold is either C^0 or C^∞ locally. In general the parameter manifold is globally C^0 and piecewise C^∞.

We assume that there exists a metric on Ω, that allows us to introduce the usual Lebesgue space $L^2(\Omega)$. In Section 5 we present in more detail the function spaces that are necessary for the analysis.

3. Mesh and mesh constraints on the parameter manifold

We introduce the general concept of a mesh $\mathcal{T}$ on a parameter manifold Ω in Section 3.1 and then develop the specific configurations we consider in Section 3.2. Following that, we present some example configurations and discuss about the meshing of complex geometries in Section 3.3.

3.1. Mesh on a parameter manifold

First we define a proto-mesh on the charts.

Definition 3. A *proto-mesh* on a proto-manifold is a collection of conforming meshes, i.e. it is a set

$$\{\tau_i\}_{i=1,\dots,N} \quad \text{with } \tau_i = \{q \subset \omega_i\}, \tag{2}$$

where

- each set τ_i is composed of open polytopes q, called *elements*; these are intervals, quadrilaterals, hexahedra, etc., depending on the dimension $d = 1, 2, 3, \dots$, respectively, and each set τ_i is a mesh on ω_i, i.e. the elements are disjoint and the union of the closures of the elements is the closure of ω_i;
- for every i, j, $\omega_{i,j}$ is the interior of the union of the closure of elements of τ_i; and
- the transition functions $\psi_{i,j}$ map elements onto elements, i.e.

$$\forall q \in \tau_i,\ \psi_{i,j}(q) \in \tau_j. \tag{3}$$

Furthermore, we have the following.

Assumption 4. The transition functions are continuous piecewise d-linear mappings with respect to the mesh.

The proto-mesh naturally defines a mesh on Ω.

Definition 5 *(Mesh on Ω).* We define the mesh on the parameter manifold Ω as

$$\mathcal{T} = \{Q \subset \Omega :\ Q = \pi_i(q), q \in \tau_i, i = 1, \dots, N\}. \tag{4}$$

Remark 2. Thanks to (3), the set $\mathcal{T}$ in (4) is indeed a well defined mesh on Ω. The elements of $\mathcal{T}$ are subsets of Ω that fulfill the standard properties of a mesh, i.e. the elements are disjoint, the union of the closures of the elements is the closure of Ω. Since Ω is a topological manifold the notion of the closure of elements, boundary edges, faces, etc. is well defined and derives from the local definition on each chart and the equivalence relation given by the transition functions.

3.2. Structured and unstructured charts on the parameter manifold

In the following we classify and restrict ourselves to specific but relevant charts, depending on their local mesh topology.

We will say that several objects *share* a common object A, if A is contained in the closure of each of the objects. Mesh objects and properties defined on the charts can be carried over to the mesh $\mathcal{T}$ on Ω. We will not distinguish between the mesh $\mathcal{T}$ on Ω and the proto-mesh defined on the charts, unless it is necessary. The relations between vertices, edges, faces and elements are stated within the global mesh. Moreover, these geometric objects are always assumed to be open.

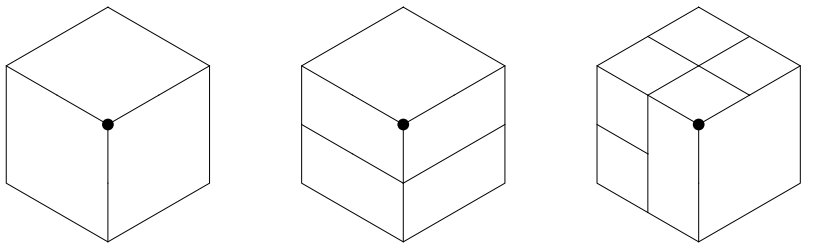

Fig. 2. Examples of meshes on a ring of three conforming segments around a two-dimensional extraordinary vertex of valence 3.

Definition 6 *(Structured chart).* A d-dimensional chart ω_i is called a *structured chart* if

(a) ω_i is a d-box, that is

$$\omega_i = \prod_{\ell=1}^{d}]a_{i,\ell}, b_{i,\ell}[,$$

and τ_i is a box mesh (see, e.g., Dokken et al., 2013);
(b) for every j, $\omega_{i,j}$ is a d-box or the union of d-boxes with disjoint closures; and
(c) for every j, if ω_j is a structured chart then the transition function $\psi_{i,j} : \omega_{i,j} \to \omega_{j,i}$ is an affine mapping (a linear polynomial) in each connected component of $\omega_{i,j}$.

Considering unstructured charts we need to distinguish three different types, depending on the dimension and on the topological structure.

Definition 7 *(Unstructured vertex chart, two-dimensional).* A two-dimensional chart ω_i is called an *unstructured vertex chart* with an associated *extraordinary vertex* $\boldsymbol{\xi}_i \in \mathbb{R}^2$ of *valence* $k_i \neq 4$ if

(a) ω_i is formed by a ring of k_i conforming quadrangular segments $s_{i,\ell}$, with $\ell = 1, \dots, k_i$, around $\boldsymbol{\xi}_i$, where each segment has a mesh $\sigma_{i,\ell}$ which is topologically equivalent to a box mesh, and the mesh τ_i is given as the union of the meshes $\sigma_{i,\ell}$;
(b) ω_i, except for the extraordinary vertex $\boldsymbol{\xi}_i$, is covered by the transition domains $\omega_{i,j}$ with structured charts, i.e.

$$\bigcup_{\substack{j=1,\dots,N \\ \omega_j \text{ structured}}} \omega_{i,j} = \omega_i \setminus \boldsymbol{\xi}_i,$$

and the transition domains $\omega_{i,j}$ are given by the union of segments; and
(c) if ω_j is an unstructured chart with $i \neq j$, then $\omega_{i,j} = \emptyset$.

To give more insight into the definition of an unstructured vertex chart via its segments, we present some example configurations, which are all constructed from the same three conforming segments. Fig. 2(a) depicts a mesh where each segment is covered by a single element. Fig. 2(b) depicts a conforming mesh and Fig. 2(c) contains two hanging vertices, hence it is a non-conforming mesh. This figure also tells that the non-conformity of the mesh over the unstructured vertex chart may have two reasons, either the meshes on two neighboring segments do not match (upper right hanging vertex) or the T-node is already present within the mesh $\sigma_{i,\ell}$ on the segment (lower left hanging vertex).

Definition 8 *(Unstructured edge chart).* A three-dimensional chart ω_i is called an *unstructured edge chart* of valence $k_i \neq 4$ if

(a) $\omega_i = \mathring{\omega}_i \times \bar{\omega}_i$, where the chart $\mathring{\omega}_i$ is a two-dimensional unstructured vertex chart, as in Definition 7 (a), with an extraordinary point $\mathring{\boldsymbol{\xi}}_i$ of valence k_i, partitioned into two-dimensional segments $\mathring{s}_{i,\ell}$ for $\ell = 1, \dots, k_i$; $\bar{\omega}_i$ is an interval $\bar{\omega}_i =]a_{i,3}, b_{i,3}[$; each three-dimensional segment $s_{i,\ell} = \mathring{s}_{i,\ell} \times \bar{\omega}_i$ has a mesh $\sigma_{i,\ell}$ which is equivalent to a three-dimensional box mesh, and the mesh τ_i is again given as the union of all meshes $\sigma_{i,\ell}$ on the segments;
(b) ω_i, except for the *extraordinary line* $\mathring{\boldsymbol{\xi}}_i \times \bar{\omega}_i$, is covered by transition domains $\omega_{i,j}$ with structured charts, i.e.

$$\bigcup_{\substack{j=1,\dots,N \\ \omega_j \text{ structured}}} \omega_{i,j} = \omega_i \setminus \mathring{\boldsymbol{\xi}}_i \times \bar{\omega}_i,$$

and the transition domains $\omega_{i,j}$ are given as the Cartesian product of the union of two-dimensional segments with an interval in the third direction;
(c) for structured charts ω_j the transition function $\psi_{i,j}$ is linear in the third coordinate ζ_3; and
(d) if ω_j is an unstructured edge chart with $i \neq j$ and $\omega_{i,j} \neq \emptyset$, then there exists a structured chart ω_k as well as an unstructured vertex chart ω_ℓ such that $\omega_{i,j} \subseteq \omega_{i,k}$ and $\omega_{i,j} \subseteq \omega_{i,\ell}$.

Definition 9 *(Unstructured vertex chart, three-dimensional).* A three-dimensional chart ω_i is called an *unstructured vertex chart* with an associated *extraordinary vertex* $\boldsymbol{\xi}_i \in \mathbb{R}^3$ of *valence* k_i if

(a) ω_i is formed by a ring of k_i conforming hexahedral segments $s_{i,\ell}$, with $\ell = 1, \dots, k_i$, around $\boldsymbol{\xi}_i$, where each segment has a mesh $\sigma_{i,\ell}$ which is topologically equivalent to a box mesh, and the mesh τ_i is given as the union of the meshes $\sigma_{i,\ell}$ on the segments $s_{i,\ell}$;
(b) ω_i, except for the extraordinary vertex $\boldsymbol{\xi}_i$, is covered by the transition domains $\omega_{i,j}$ with structured charts or unstructured edge charts, i.e.,

$$\bigcup_{\substack{j=1,\dots,N \\ \omega_j \text{ structured or unstructured edge chart}}} \omega_{i,j} = \omega_i \setminus \boldsymbol{\xi}_i,$$

and the transition domains $\omega_{i,j}$ are given by the union of segments; and
(c) if ω_j is an unstructured vertex chart with $i \neq j$, then $\omega_{i,j} = \emptyset$.

Note that from Definition 8(b) and Definition 9(b) it follows that for every unstructured vertex chart in 3D the transition domains with structured charts cover everything, except for the extraordinary features (union of extraordinary vertex and extraordinary edges). In particular, the interior of every element is covered.

Remark 3. We would like to point out that Definitions 7(c), 8(d) and 9(c) are not strictly necessary, but technicalities to simplify the definition of spline manifold spaces in Section 4. The conditions in Definitions 7(c) and 9(c) guarantee that unstructured vertex charts do not overlap. Considering Definition 8(d), the set $\omega_{i,j}$ forms a structured mesh (i.e. it does not contain extraordinary features in its interior). Therefore, the condition $\omega_{i,j} \subseteq \omega_{i,k}$ for some structured chart Ω_k is natural. Moreover, unstructured edge charts cover unstructured edges, which meet at unstructured vertices. Hence, we assume that whenever two unstructured edge charts overlap, there exists an unstructured vertex chart covering the intersection.

Notice that it is not possible that one element of the mesh $\mathcal{T}$ is adjacent to two unstructured vertices. In the context of meshing, this is not a severe restriction as we point out in the following section. Moreover, each unstructured vertex and each unstructured edge correspond to exactly one unstructured vertex chart or unstructured edge chart, respectively.

Assumption 10. We assume that each chart ω_i can be either structured as in Definition 6 or unstructured as in Definitions 7, 8 and 9.

In the following section we give some example configurations and study in more detail the meshing of complex geometries.

3.3. Example configurations and meshing of complex geometries

For simplicity, in the classification above we have restricted ourselves to a limited number of types of charts, which nevertheless contain most mesh configurations of practical interest. We first give a summary of the different types of vertices that can occur (depending on the dimension), which motivates our chart classification. Each unstructured chart is formally defined in such a way, that it can be used to cover a certain type of unstructured vertex. Following the discussion of the types of vertices, we present some simple example configurations and discuss the issues of meshing with manifolds. Without being thorough, we present the configurations that can be covered in our framework. Since we do not want to go into the details of meshing we refer to the following literature for quad-meshing (Owen, 1998) and hex-meshing (Owen, 1998; Jüttler et al., 2014; Nguyen et al., 2014a).

3.3.1. Classification of vertices and edges

For 1D domains (intervals, planar or spatial curves) there are only regular vertices, which are equivalent to the knots in the classical B-spline language. Hence no unstructured charts are needed.

For 2D domains we consider three types of vertices. A 2D vertex can be a *regular vertex*, a *hanging vertex* (a T-node), or an *extraordinary vertex* (see Table 1 and Fig. 3). Both regular and hanging vertices are covered by structured charts, although they may also belong to an unstructured chart. Unstructured vertex charts cover a neighborhood of an extraordinary vertex.

Table 1
Classification of vertices in 2D.

Structured vertex	Regular vertex	(Fig. 3(a))
	Hanging vertex	(Fig. 3(b))
Unstructured vertex	Extraordinary vertex	(Figs. 3(c) and 3(d))

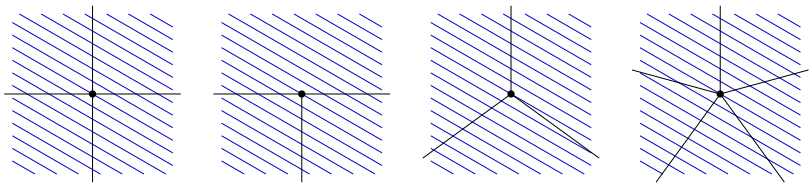

Fig. 3. Different types of vertices in 2D ((a) regular, (b) hanging, (c) extraordinary of valence 3, (d) extraordinary of valence 5).

Table 2
Classification of edges and vertices in 3D.

Structured edge	Regular edge
	Hanging edge
Unstructured edge	Extraordinary edge
Structured vertex	Regular vertex
	Hanging vertex
Unstructured vertex	Partially unstructured vertex
	Fully unstructured vertex

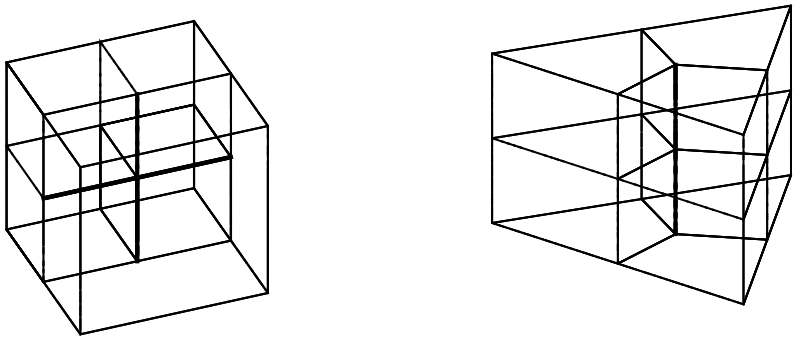

Fig. 4. Examples of the different types of edges. Interior edges not highlighted are regular edges.

For 3D domains we have three types of edges and four types of vertices. A 3D edge can be a *regular edge*, a *hanging edge*, as in Fig. 4(a), or an *extraordinary edge* of valence $k \neq 4$ as in Fig. 4(b), where the highlighted edges have valence $k = 3$. A 3D vertex is called a *regular vertex*, if it is shared by regular edges only; or a *hanging vertex*, if it is shared by regular and hanging edges. Otherwise, the vertex is called an unstructured vertex. The notion of unstructured vertices contains both vertices of extraordinary edges, so called *partially unstructured vertices*, as well as *fully unstructured vertices*. To be precise, a partially unstructured vertex is a vertex that is shared by exactly two extraordinary edges that can be covered by a single unstructured edge chart. If this is not possible, the vertex is a fully unstructured vertex. For a complete list of types of vertices and edges in 3D see Table 2. Regular and hanging edges as well as regular and hanging vertices are covered by structured charts. Hence, we have considered two classes of three-dimensional unstructured charts: unstructured vertex charts (covering fully unstructured vertices) and unstructured edge charts (covering partially unstructured vertices and extraordinary edges). Unstructured edge charts are Cartesian products of an unstructured vertex chart in two dimensions and an interval in the third dimension: there is an inner sequence of extraordinary edges and all other interior edges are either regular or hanging. Similar to the two-dimensional case, an unstructured vertex chart in 3D covers a neighborhood of the fully unstructured vertex.

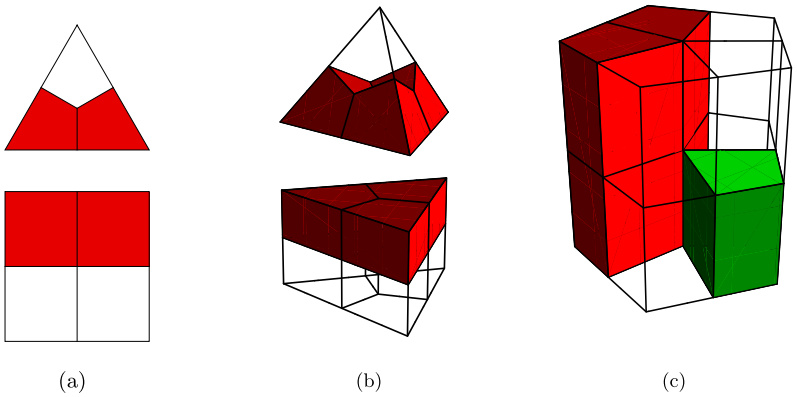

Fig. 5. Different types of unstructured charts.

3.3.2. Example configurations

Let us consider an unstructured vertex chart ω_i composed of k_i segments, where each segment is meshed with only one element. From Definition 6 it follows that for any structured chart ω_j with $\omega_{i,j} \neq \emptyset$ the transition domain $\psi_{i,j}(\omega_{i,j}) = \omega_{j,i}$ is a box-mesh. The same holds for $\omega_{i,j}$, which is then formed by one or at most two quadrilateral elements. There must be (at least) k_i subsets $\omega_{i,j}$, each one formed by two adjacent elements, in order to cover $\omega_i \setminus \boldsymbol{\xi}_i$.

Fig. 5(a) depicts a two-dimensional unstructured vertex chart ω_i of valence 3 and a structured chart, as well as the corresponding transition domains. Since the transition domains are open, it can be observed easily, that in this case three structured charts are needed to cover ω_i, except the extraordinary vertex. Fig. 5(b) depicts a three-dimensional unstructured vertex chart ω_i of valence 4 as well as an unstructured edge chart of valence 3 and corresponding transition domains. Again, we may observe that ω_i (except for the extraordinary vertex) can be covered by the transition domains of four unstructured edge charts. Moreover, ω_i (except for the extraordinary vertex and edges) can be covered with six structured charts. Fig. 5(c) depicts an unstructured edge chart of valence 5 and two possible transition domains. Note that all the transition domains are mapped box-meshes, due to the definitions above. In all the examples presented here we assume that for each unstructured vertex chart each segment is meshed with exactly one element. This is not necessarily the case, as we presented in Fig. 2. Note that, by definition, the transition domains with structured charts can cover no more than two segments of an unstructured chart.

3.3.3. Meshing

Note that the types of charts we consider are sufficient to represent most meshes of practical interest. Given an arbitrary quad- or hex-mesh without hanging vertices or edges, a global bisection of the mesh can be covered by structured charts, as in Definition 6, and unstructured charts, as in Definitions 7, 8 and 9.

This statement becomes clear when looking at the types of vertices and edges that can occur in the bisected mesh. We consider only 3D meshes in the following. We show that every vertex of the bisected mesh can be covered by a valid chart of one of the three categories. Every vertex of the initial hex-mesh is one of the three: a structured vertex, a partially unstructured vertex or a fully unstructured vertex. The bisection of the initial mesh introduces new vertices from midpoints of edges, faces and hex-elements (one point for each edge, face and element). The midpoints of structured edges, faces and elements become structured vertices. The midpoints of unstructured edges become partially unstructured vertices. Hence no new fully unstructured vertices are introduced. All structured vertices can be covered by structured charts, all partially unstructured vertices can be covered by unstructured edge charts and all fully unstructured vertices can be covered by unstructured vertex charts. It is easy to see that, due to the bisection, the closure of any element can contain at most one extraordinary vertex. All other assumptions are trivially fulfilled.

4. Spline manifold space on the parameter manifold

In this section we introduce spline spaces over the mesh $\mathcal{T}$ on Ω, in short *spline manifold spaces*.

4.1. General spline manifold spaces

Again based on Grimm and Hughes (1995), we define a spline space on a parameter manifold using the charts. This is achieved by defining proto-basis functions on the proto-mesh (Definition 11) and transferring them onto the parameter manifold using the equivalence relation induced by the transition functions (Definition 13). Each chart ω_i plays the role of a local parameter domain.

Definition 11 *(Proto-basis functions).* For each $i = 1, \ldots, N$, let

$$\left\{b_{\mathbf{A}_i} : \omega_i \to \mathbb{R}\right\}_{\mathbf{A}_i \in \mathcal{A}_i} \tag{5}$$

be a given *local basis* on the chart ω_i such that each function $b_{\mathbf{A}_i}$ fulfills

$$\lim_{\boldsymbol{\zeta} \to \partial\omega_i} b_{\mathbf{A}_i}(\boldsymbol{\zeta}) = 0. \tag{6}$$

The collection of all these local bases for $i = 1, \dots, N$ is called a *proto-basis*.

Assumption 12. The proto-basis functions $b_{\mathbf{A}_i}$ with $\mathbf{A}_i \in \mathcal{A}_i$ are piecewise polynomials with respect to τ_i, i.e. $b_{\mathbf{A}_i}|_q$ is polynomial for all $q \in \tau_i$.

Definition 13 *(Spline manifold space).* For each $i = 1, \dots, N$ and $\mathbf{A}_i \in \mathcal{A}_i$ we define $B_{\mathbf{A}_i} : \Omega \to \mathbb{R}$ such that

$$\begin{aligned} B_{\mathbf{A}_i}|_{\Omega_i} &= b_{\mathbf{A}_i} \circ \pi_i^{-1} \\ B_{\mathbf{A}_i}|_{\Omega \setminus \Omega_i} &= 0, \end{aligned} \tag{7}$$

and set

$$\mathcal{B}_i = \{B_{\mathbf{A}_i} : \Omega \to \mathbb{R}, \mathbf{A}_i \in \mathcal{A}_i\}. \tag{8}$$

Furthermore, we introduce the global index set

$$\mathcal{A} = \left(\bigsqcup_{i=1,\dots,N} \mathcal{A}_i \right) \Big/ \approx \tag{9}$$

where the equivalence relation $\approx$ is defined as follows: given $[\mathbf{A}_i, i]$ and $[\mathbf{A}_j, j]$ in $\bigsqcup_{i=1,\dots,N} \mathcal{A}_i$, then $[\mathbf{A}_i, i] \approx [\mathbf{A}_j, j]$ if and only if the two functions $B_{\mathbf{A}_i} \in \mathcal{B}_i$ and $B_{\mathbf{A}_j} \in \mathcal{B}_j$ coincide. Therefore, $B_{\mathbf{A}} : \Omega \to \mathbb{R}$ is well defined for $\mathbf{A} \in \mathcal{A}$, and we set

$$\mathcal{B} = \{B_{\mathbf{A}}, \mathbf{A} \in \mathcal{A}\} \equiv \bigcup_{i=1,\dots,N} \mathcal{B}_i. \tag{10}$$

Finally, we set

$$\tilde{\mathcal{B}}_i = \{B_{\mathbf{A}}|_{\Omega_i}, \mathbf{A} \in \tilde{\mathcal{A}}_i\}, \tag{11}$$

where

$$\tilde{\mathcal{A}}_i = \{\mathbf{A} \in \mathcal{A} : \operatorname{supp}(B_{\mathbf{A}}) \cap \operatorname{supp}(B_{\mathbf{A}_i}) \neq \emptyset \text{ for some } \mathbf{A}_i \in \mathcal{A}_i\}. \tag{12}$$

The set $\tilde{\mathcal{B}}_i$ is the restriction of $\mathcal{B}$ onto Ω_i containing all the functions in $\mathcal{B}_i$ and also the restriction of any function whose support intersects $\operatorname{supp}(\mathcal{B}_i)$ but is not included in $\mathcal{B}_i$. The functions in $\tilde{\mathcal{B}}_i$ can be pulled back to the chart ω_i. Finally, the span of functions in (10) is the *spline manifold space*, the spline space on the parameter manifold Ω, denoted by

$$\mathcal{S} = \operatorname{span}\{B_{\mathbf{A}}, \mathbf{A} \in \mathcal{A}\}. \tag{13}$$

With some abuse of notation, for the global index $\mathbf{A} \in \mathcal{A}$ we will say that $\mathbf{A} \in \mathcal{A}_i$ if there exists an index $\mathbf{A}_i \in \mathcal{A}_i$ such that its equivalence class $[\mathbf{A}_i, i]$ through $\approx$ is equal to $\mathbf{A}$.

Assumption 14. For each $i = 1, \dots, N$ and each $\mathbf{A} \in \mathcal{A}$ we have that if

$$\operatorname{supp}(B_{\mathbf{A}}) \subseteq \Omega_i$$

then $\mathbf{A} \in \mathcal{A}_i$; furthermore we assume

$$\bigcup_{\mathbf{A}_i \in \mathcal{A}_i} \operatorname{supp}(B_{\mathbf{A}_i}) = \Omega_i. \tag{14}$$

Remark 4. Equation (6) together with (7) guarantees that the functions are globally continuous. If one wants to allow for discontinuous functions, the condition (6) can be omitted.

4.2. B-Spline manifold spaces

In this section we characterize the B-spline functions as structured and unstructured (of edge or vertex type) ones. To classify them, we introduce the notation

$$\begin{aligned}
\mathcal{A}_s &= \bigcup_{i\,:\,\omega_i \text{ is structured}} \mathcal{A}_i, \\
\mathcal{A}_e &= \left(\bigcup_{i\,:\,\omega_i \text{ is unstr. edge}} \mathcal{A}_i \right) \setminus \mathcal{A}_s, \\
\mathcal{A}_v &= \left(\bigcup_{i\,:\,\omega_i \text{ is unstr. vertex}} \mathcal{A}_i \right) \setminus (\mathcal{A}_s \cup \mathcal{A}_e),
\end{aligned} \tag{15}$$

and we will call $\mathcal{A}_s$ the index set of structured functions, $\mathcal{A}_e$ the index set of edge (or partially) unstructured functions and $\mathcal{A}_v$ the index set of vertex (or fully) unstructured functions. It is clear that

$$\mathcal{A}_s \cap \mathcal{A}_e = \mathcal{A}_s \cap \mathcal{A}_v = \mathcal{A}_e \cap \mathcal{A}_v = \emptyset. \tag{16}$$

In the following we do not distinguish between the two- and three-dimensional case. Since unstructured edge charts do not exist in 2D, we simply set $\mathcal{A}_e = \emptyset$ in that case.

Hence we conclude that the set $\mathcal{B}_i$ contains all functions that are completely supported in Ω_i and by (12) and (14) the set $\tilde{\mathcal{B}}_i$ contains all functions that have a support intersecting with Ω_i.

For simplicity we assume that the functions have the same degree p in each direction on each structured chart.

Assumption 15. If ω_i is a structured chart as in Definition 6, then each function $B_{\mathbf{A}}$ in $\tilde{\mathcal{B}}_i$ is a tensor-product B-spline of degree p when restricted to ω_i, i.e., there exist (local) knot vectors $\Xi_{\mathbf{A},i,1}, \dots, \Xi_{\mathbf{A},i,d}$ such that

$$B_{\mathbf{A}} \circ \pi_i(\boldsymbol{\zeta}) = b[\Xi_{\mathbf{A},i,1}](\zeta_1) \dots b[\Xi_{\mathbf{A},i,d}](\zeta_d), \qquad \forall \mathbf{A} \in \tilde{\mathcal{A}}_i, \forall \boldsymbol{\zeta} \in \omega_i, \tag{17}$$

where $b[\Xi](\zeta)$ is the univariate B-spline with local knot vector Ξ. Moreover, if the support of a function $B_{\mathbf{A}}$ is structured, then there exists a structured chart that covers the support.

Finally, the previous assumption is extended to unstructured edge charts, since they behave like structured charts along the third parametric direction, and like unstructured vertex charts along the first two parametric directions.

Assumption 16. If ω_i is an unstructured edge chart as in Definition 8, then each function $B_{\mathbf{A}}$ in $\tilde{\mathcal{B}}_i$ is a product of a bivariate function and a B-spline of degree p in ζ_3 when restricted to ω_i, i.e. there exist a function $\beta_{\mathbf{A},i}$ and a local knot vector $\Xi_{\mathbf{A},i,3}$ such that

$$B_{\mathbf{A}} \circ \pi_i(\boldsymbol{\zeta}) = \beta_{\mathbf{A},i}(\zeta_1, \zeta_2) b[\Xi_{\mathbf{A},i,3}](\zeta_3), \qquad \forall \mathbf{A} \in \tilde{\mathcal{A}}_i, \forall \boldsymbol{\zeta} \in \omega_i. \tag{18}$$

Remark 5. From the definition of the unstructured charts ω_j, and under Assumption 15, we have that the functions $B_{\mathbf{A}}$, with $\mathbf{A} \in \mathcal{A}_j$, are fully defined by their restrictions to the transition domains $\omega_{j,i}$ with structured charts. On each $\omega_{j,i}$ the functions in $\mathcal{B}_j \cap \tilde{\mathcal{B}}_i$ are equivalent to (mapped) tensor-product B-splines according to (17). Notice that in practice this limits the possible definitions of unstructured functions, but less restrictive versions of Assumption 15 can be introduced to deal with other configurations.

4.3. Isogeometric function spaces using spline manifolds

We consider a domain $\Sigma \subset \mathbb{R}^n$ which can be interpreted as a d-dimensional manifold with $d \leq n$. The most interesting cases, and the ones we focus on, are a two-dimensional planar domain $\Sigma \subset \mathbb{R}^2$, a surface $\Sigma \subset \mathbb{R}^3$ or a three-dimensional volumetric domain $\Sigma \subset \mathbb{R}^3$.

Definition 17. $\Sigma \in \mathbb{R}^n$ is a *spline manifold domain*

$$\mathbf{G} : \Omega \to \Sigma \tag{19}$$

where Ω is a (spline) parameter manifold and $\mathbf{G} \in (\mathcal{S})^n$ a *spline manifold parametrization*.

In practical situations, this parametrization is defined by associating a control point to each function in $\mathcal{B}$. Notice that the geometry Σ inherits the manifold structure of the parameter manifold Ω. Indeed, the parametrization $\mathbf{G}$ can be considered as a piecewise defined function, where $\mathbf{G}_i : \Omega_i \to \Sigma_i$ is a tensor-product B-spline (or structured T-spline) parametrization for every structured chart Ω_i. Then we have

$$\Sigma = \bigcup_{i=1}^{N} \Sigma_i,$$

where the charts Σ_i form an *atlas* of Σ.

Then, the isogeometric function space over the manifold Σ is given as follows.

Definition 18. Given a *spline manifold parametrization* $\mathbf{G} \in (\mathcal{S})^n$ as in Definition 17, we define on the spline manifold domain Σ the *isogeometric function space* as

$$\mathcal{V} = \{f : \Sigma \to \mathbb{R}, \text{ such that } f = \hat{f} \circ \mathbf{G}^{-1} \text{ for } \hat{f} \in \mathcal{S}\}. \tag{20}$$

The isogeometric space is well-defined, if the geometry parametrization is invertible.

Similar to the spline manifold space $\mathcal{S}$ itself, the isogeometric space $\mathcal{V}$ can be interpreted as a piecewise defined function space. Indeed, each function in $\mathcal{B}_i$ can be composed with $\mathbf{G}^{-1}$ to define the corresponding function in Σ, with its support contained in the chart Σ_i.

4.4. Relation to existing constructions

We note that several constructions of unstructured spline spaces existing in the literature fit in the framework of B-spline manifolds, in some cases with minor modifications. For instance, the definition of multi-patch B-splines with enhanced smoothness as developed in Buchegger et al. (2015), the G^1-smooth multi-patch constructions as in Groisser and Peters (2015), Kapl et al. (2015b), Collin et al. (2015), or unstructured T-splines as presented in Wang et al. (2011, 2012) for quad-meshes and hex-meshes, as well as the G^1-smooth unstructured T-splines as presented in Scott et al. (2013). The development of an abstract framework for the construction of these spaces can serve as the starting point for a deeper mathematical analysis of their properties. In the following we detail how these four particular examples fit into the framework of B-spline manifolds. In any case, the idea is to split the set of basis functions into structured and unstructured basis functions, and introduce a set of charts covering the whole mesh. In this context, and recalling the definition of the index sets in (15), a function is called structured if its support is covered by a structured mesh (possibly with hanging nodes). Otherwise it is called unstructured.

Multi-patch B-splines with enhanced smoothness (Buchegger et al., 2015) The authors propose a construction based on a multi-patch representation of the domain. This can be interpreted as a manifold structure with closed charts (patches), that intersect only at the boundary. However, since there is a one-to-one correspondence of parameter directions along any shared boundary between two patches, the multi-patch representation can be transformed naturally to a parameter manifold representation by simply enlarging the patches along the parameter direction crossing the boundary to obtain open charts. Note that in general it is necessary to define more than one chart to cover one patch. Again, there are unstructured functions at the extraordinary vertices, and unstructured vertex charts have to be introduced to cover their support.

G^1-smooth multi-patch B-splines (Groisser and Peters, 2015; Kapl et al., 2015b; Collin et al., 2015) The constructions developed here are based on a C^0-continuous multi-patch representation of the domain. Additional geometric continuity conditions are imposed in physical space. Hence, the resulting functions are linear combinations of tensor-product B-splines that are G^1-smooth with respect to the physical coordinates. In Groisser and Peters (2015) higher order smoothness is also discussed. This results in both special (unstructured) G^1-smooth functions at the extraordinary vertices as well as special (structured) G^1-smooth functions along the edges (see Kapl et al., 2015b). Assumption 15 has to be relaxed in order to include these special functions as well. As in the C^0-case, unstructured vertex charts have to be introduced to cover the support of the unstructured vertex functions. The geometric continuity conditions can also be incorporated implicitly as linear conditions that need to be satisfied.

T-splines over unstructured meshes (Wang et al., 2011) In this configuration the mesh $\mathcal{T}$ we consider on Ω is the Bézier mesh corresponding to the T-splines and not the T-mesh. Then, we can define the set of charts by taking the support of each structured function as a single structured chart, while the support of each unstructured function is taken as one unstructured vertex chart. In the construction of Wang et al. (2011) it may happen that one element contains two extraordinary vertices. In this case two unstructured vertex charts overlap, violating Definition 7(c). This condition is a technicality which simplifies the mathematical framework, and could be removed. It can also be fulfilled with one level of refinement of the T-mesh, as we explained in Section 3.3. In a similar way, the constructions for trivariate functions as presented in Wang et al. (2012) fit, with some technical restrictions, into the present framework.

G^1-smooth T-splines over unstructured meshes (Scott et al., 2013) This construction is similar to the construction in Wang et al. (2011). The support of each structured function can again be interpreted as a single structured chart. For each extraordinary vertex we can define one sufficiently large unstructured chart ω_j, such that it covers the support of all functions that are non-zero at the extraordinary vertex. In this case the degree of the unstructured functions is increased in the vicinity of the extraordinary vertex, and their restriction to a structured chart is not a B-spline basis function as in (17), but a suitable linear combination of B-splines of higher degree. Therefore, as for the G^1-smooth multi-patch configurations, Assumption 15 has to be relaxed in order to accomodate the unstructured functions.

5. Analysis-suitable spline manifold spaces

We introduce in this section the conditions for the construction of analysis-suitable B-spline spaces on manifolds, that is, spaces that have good properties for the solution of differential problems. The key tool for this construction is the definition of a (stable) dual basis, which is a set of functionals $\{\Lambda_{\mathbf{A}}, \mathbf{A} \in \mathcal{A}\}$ such that

$$\Lambda_{\mathbf{A}}(B_{\mathbf{A}'}) = \delta_{\mathbf{A}\mathbf{A}'}, \quad \forall \mathbf{A}, \mathbf{A}' \in \mathcal{A},$$

where $\delta_{\mathbf{A}\mathbf{A}'}$ represents the Kronecker delta. A condition for the construction of a dual basis for structured T-splines was given in Beirão da Veiga et al. (2012a, 2013), under the name of *dual-compatibility*.

We present the construction of dual functionals on the parameter manifold Ω in Section 5.1, starting from a proto-dual basis on each chart, and then following the scheme of spline manifold spaces introduced in Section 4.1. To guarantee that these dual functionals form a dual basis we need to add some conditions to the spline manifold. In Section 5.2 we give a *dual-compatibility* condition for spline manifolds, which generalizes the condition in Beirão da Veiga (2012a, 2013) to the unstructured setting. In this configuration, a global dual basis can be derived from the proto-dual bases defined on the charts. Then, in Section 5.3 we present an explicit configuration, with a specific construction of the proto-basis functions and the proto-dual basis on unstructured vertex and edge charts. In this configuration, which is only C^0-continuous at extraordinary features, the dual functionals in Ω can be derived from the proto-dual basis without any further modification, which also guarantees the stability of the dual functionals. Finally, in Section 5.4 we show the typical application of a dual basis: we prove optimal approximation properties of the isogeometric space on a simple but interesting example configuration.

5.1. The dual basis for spline manifold spaces

In the following we use this well-known fact.

Lemma 1. *Given a set of finitely many L^2 functions $\{b_\alpha\}$ that are linearly independent, there exist functionals $\lambda_\alpha : L^2 \to \mathbb{R}$ that are dual to the functions, i.e., $\lambda_\alpha(b_{\alpha'}) = \delta_{\alpha\alpha'}$.*

As for the definition of the basis functions for spline manifold spaces introduced in Section 4.1, the starting point is a set of dual-functionals on each chart, that exist thanks to the previous proposition and Definition 11.

Definition 19 *(Proto-dual basis).* For each $i = 1, \dots, N$, let the functionals

$$\{\hat{\lambda}_{\mathbf{A}_i} : L^2(\omega_i) \to \mathbb{R}\}_{\mathbf{A}_i \in \mathcal{A}_i}$$

form a *local dual basis* with the proto-basis functions in the chart, that is,

$$\hat{\lambda}_{\mathbf{A}_i}(b_{\mathbf{A}'_i}) = \delta_{\mathbf{A}_i\mathbf{A}'_i}, \quad \forall \mathbf{A}_i, \mathbf{A}'_i \in \mathcal{A}_i.$$

The collection of all these local dual bases for $i = 1, \dots, N$ is called a *proto-dual basis*.

Note that the existence of a proto-dual basis is guaranteed by Lemma 1, since the proto-basis functions $b_{\mathbf{A}_i}$ are linearly independent by Definition 11. We will assume that the proto-dual functionals satisfy the following.

Assumption 20. For any indices $[\mathbf{A}_i, i] \approx [\mathbf{A}_j, j]$ that belong to the same equivalence class $\mathbf{A} \in \mathcal{A}$, defined as in (9), it holds that $\hat{\lambda}_{\mathbf{A}_i}(\phi \circ \pi_i) = \hat{\lambda}_{\mathbf{A}_j}(\phi \circ \pi_j), \ \forall \phi \in L^2(\Omega)$.

The assumption that two equivalent indices are associated to the same dual functional is natural, since by (9) they are also associated to the same basis function, and it allows the following global definition.

Definition 21 *(Manifold functionals).* For any $\mathbf{A} \in \mathcal{A}$ we define the functional

$$\hat{\Lambda}_{\mathbf{A}}(\phi) = \hat{\lambda}_{\mathbf{A}_i}(\phi \circ \pi_i), \quad \forall \phi \in L^2(\Omega), \tag{21}$$

where $[\mathbf{A}_i, i]$ is one instance of the equivalence class $\mathbf{A}$.

From (21), the support of the dual functional $\hat{\Lambda}_{\mathbf{A}}$ is contained in Ω_i. The most used dual bases for splines, such as the one by Schumaker (2007) and the ones by Lee et al. (2001) satisfy the stronger condition that the support of $\hat{\Lambda}_{\mathbf{A}}$ is the same as the support of the corresponding function $B_{\mathbf{A}}$.

Note that in general the dual functionals $\{\hat{\Lambda}_{\mathbf{A}}, \mathbf{A} \in \mathcal{A}\}$ do not form a dual basis for $\mathcal{B} = \{B_{\mathbf{A}}, \mathbf{A} \in \mathcal{A}\}$. In the following section we introduce a new condition that ensures that a dual basis can be derived by a modification of the dual functionals $\hat{\Lambda}_{\mathbf{A}}$.

5.2. Dual-compatible spline manifold spaces

For the definition of the dual-compatibility condition we follow and extend the recent review paper (Beirão da Veiga et al., 2014). Two knot vectors $\Xi' = \{\xi'_1, \dots, \xi'_{p+2}\}$ and $\Xi'' = \{\xi''_1, \dots, \xi''_{p+2}\}$ *overlap* if there exists a knot vector $\Xi = \{\xi_1, \dots, \xi_k\}$ and two integers k' and k'' such that $\xi'_i = \xi_{i+k'}$ and $\xi''_i = \xi_{i+k''}$, for $i = 1, \dots, p+2$. We generalize the dual-compatibility condition to spline manifold spaces in the following definition.

Definition 22 *(Dual-compatible spline manifold spaces).* Under the previously stated assumptions, the set $\mathcal{B}$ defined in (10) is dual-compatible if the following conditions hold

(a) for all $\mathbf{A} \in \mathcal{A}_i \subset \mathcal{A}_s$ and $\forall \mathbf{A}' \in \widetilde{\mathcal{A}}_i$, with $\mathbf{A} \neq \mathbf{A}'$, there exists an index $l \in \{1, \dots, d\}$, such that the knot vectors $\Xi_{\mathbf{A},i,l}$ and $\Xi_{\mathbf{A}',i,l}$ as in (17) are different and overlap;
(b) for all $\mathbf{A} \in \mathcal{A}_i \cap \mathcal{A}_e$, with ω_i being an unstructured edge chart, and for all $\mathbf{A}' \in \mathcal{A}_i$, with $\mathbf{A} \neq \mathbf{A}'$, either the knot vectors $\Xi_{\mathbf{A},i,3}$ and $\Xi_{\mathbf{A}',i,3}$ as in (18) overlap and are different, or $\beta_{\mathbf{A},i} \neq \beta_{\mathbf{A}',i}$;
(c) for all $\mathbf{A} \in \mathcal{A}_i \cap \mathcal{A}_e$, with ω_i being an unstructured edge chart, and for all $\mathbf{A}' \in (\widetilde{\mathcal{A}}_i \setminus \mathcal{A}_i) \cap (\mathcal{A}_e \cup \mathcal{A}_v)$ the knot vectors $\Xi_{\mathbf{A},i,3}$ and $\Xi_{\mathbf{A}',i,3}$ as in (18) overlap and are different.

Here $\mathcal{A}_s$, $\mathcal{A}_e$ and $\mathcal{A}_v$ are defined as in (15).

In Definition 22(b) both $B_{\mathbf{A}}$ and $B_{\mathbf{A}'}$ are unstructured edge functions from the same unstructured edge chart. In 22(c) $B_{\mathbf{A}}$ is an unstructured edge function and $B_{\mathbf{A}'}$ is an unstructured function from a different chart.

In Beirão da Veiga et al. (2014) (as well as the previous papers (Beirão da Veiga et al. 2012a, 2013)) the authors deal only with the structured case, and actually the dual-compatibility condition in Beirão da Veiga et al. (2014) corresponds to point (a) in Definition 22. The new definition extends the dual-compatibility condition to an unstructured configuration. As in Beirão da Veiga et al. (2014), Definition 22 gives a sufficient condition for the existence of a dual basis. For that, we use two technical ingredients: the first is a univariate L^2-stable dual functional $\lambda[\Xi]$, such that, if Ξ and Ξ' are overlapping,

$$\lambda[\Xi](b[\Xi']) = \begin{cases} 1 & \text{if } \Xi = \Xi', \\ 0 & \text{if } \Xi \neq \Xi'; \end{cases} \tag{22}$$

see, for example, Schumaker (2007), Lee et al. (2001); the second is the existence of a proto-dual basis on each chart, guaranteed by Lemma 1. Our main result follows.

Theorem 2. *If the set $\mathcal{B}$ is dual-compatible, then there exists a set of functionals*

$$\mathcal{B}^* = \left\{ \Lambda_{\mathbf{A}} : L^2(\Omega) \to \mathbb{R} \text{ such that } \mathbf{A} \in \mathcal{A} \right\},$$

that is dual to $\mathcal{B}$, i.e.,

$$\forall \mathbf{A}, \mathbf{A}' \in \mathcal{A},\ \Lambda_{\mathbf{A}}(B_{\mathbf{A}'}) = \delta_{\mathbf{A}\mathbf{A}'}. \tag{23}$$

Proof. First, we construct dual functionals for the different types of charts. Let ω_i be a structured chart. Given $\mathbf{A} \in \mathcal{A}_i \subset \mathcal{A}_s$ we set

$$\hat{\lambda}_{\mathbf{A}} = \lambda[\Xi_{\mathbf{A},i,1}] \otimes \dots \otimes \lambda[\Xi_{\mathbf{A},i,d}], \tag{24}$$

where the knot vectors $\Xi_{\mathbf{A},i,k}$ are given as in (17). Let ω_i be an unstructured edge chart. Given $\mathbf{A} \in \mathcal{A}_i \cap \mathcal{A}_e$, let $\mathcal{A}_{i,\mathbf{A}} \subset \mathcal{A}_i \cap \mathcal{A}_e$ be the set of indices $\mathbf{A}'$ such that $\Xi_{\mathbf{A},i,3} = \Xi_{\mathbf{A}',i,3}$ as in (18). Since the set $\mathcal{B}_i$ is linearly independent, the same holds for the set

$$\{\beta_{\mathbf{A}',i} : \mathbf{A}' \in \mathcal{A}_{i,\mathbf{A}}\} \tag{25}$$

and by Lemma 1 there exist functionals $\{\hat{\lambda}_{\mathbf{A}',i} : \mathbf{A}' \in \mathcal{A}_{i,\mathbf{A}}\}$ that are dual to (25). We define the proto-dual functional $\hat{\lambda}_{\mathbf{A}} : \omega_i \to \mathbb{R}$

$$\hat{\lambda}_{\mathbf{A}} = \hat{\lambda}_{\mathbf{A},i} \otimes \lambda[\Xi_{\mathbf{A},i,3}].$$

Finally, let ω_i be an unstructured vertex chart. Consider $\mathcal{A}_i \cap \mathcal{A}_v$, and again by Lemma 1 the set $\mathcal{B}_i$, which is assumed to be linearly independent, admits a proto-dual basis $\{\hat{\lambda}_{\mathbf{A}} : \mathbf{A} \in \mathcal{A}_i \cap \mathcal{A}_v\}$. Having defined $\lambda_{\mathbf{A}}$ for all $\mathbf{A} \in \mathcal{A}$, we construct the corresponding $\hat{\Lambda}_{\mathbf{A}}$ as in (21).

It is easy to check that, by the construction above and Definition 22, it holds

$$\forall \mathbf{A} \in \mathcal{A}_s, \forall \mathbf{A}' \in (\mathcal{A}_s \cup \mathcal{A}_e \cup \mathcal{A}_v), \quad \hat{\Lambda}_{\mathbf{A}}(B_{\mathbf{A}'}) = \delta_{\mathbf{A}\mathbf{A}'}, \tag{26}$$

$$\forall \mathbf{A} \in \mathcal{A}_e, \forall \mathbf{A}' \in (\mathcal{A}_e \cup \mathcal{A}_v), \quad \hat{\Lambda}_{\mathbf{A}}(B_{\mathbf{A}'}) = \delta_{\mathbf{A}\mathbf{A}'}, \tag{27}$$

$$\forall \mathbf{A} \in \mathcal{A}_v, \forall \mathbf{A}' \in \mathcal{A}_v, \quad \hat{\Lambda}_{\mathbf{A}}(B_{\mathbf{A}'}) = \delta_{\mathbf{A}\mathbf{A}'}. \tag{28}$$

From Definition 21 we can also infer

$$\forall \mathbf{A} \in \mathcal{A}, \forall \mathbf{A}' \in \mathcal{A} \setminus \tilde{\mathcal{A}}_i, \quad \hat{\Lambda}_{\mathbf{A}}(B_{\mathbf{A}'}) = 0. \tag{29}$$

In general, the set of functionals $\{\hat{\Lambda}_{\mathbf{A}}\}_{\mathbf{A}\in\mathcal{A}}$ is not dual to the set of functions $\mathcal{B} = \{B_{\mathbf{A}}\}_{\mathbf{A}\in\mathcal{A}}$, but we can easily fix it by defining, for all $\phi \in L^2(\Omega)$, the functionals:

$$\begin{aligned}
&\forall \mathbf{A} \in \mathcal{A}_s, \Lambda_{\mathbf{A}}(\phi) = \hat{\Lambda}_{\mathbf{A}}(\phi), \\
&\forall \mathbf{A} \in \mathcal{A}_e, \Lambda_{\mathbf{A}}(\phi) = \hat{\Lambda}_{\mathbf{A}}(\phi) - \sum_{\mathbf{A}'' \in (\tilde{\mathcal{A}}_i \setminus \mathcal{A}_i) \cap \mathcal{A}_s} \hat{\Lambda}_{\mathbf{A}}(B_{\mathbf{A}''})\Lambda_{\mathbf{A}''}(\phi), \\
&\forall \mathbf{A} \in \mathcal{A}_v, \Lambda_{\mathbf{A}}(\phi) = \hat{\Lambda}_{\mathbf{A}}(\phi) - \sum_{\mathbf{A}'' \in \tilde{\mathcal{A}}_i \setminus \mathcal{A}_i} \hat{\Lambda}_{\mathbf{A}}(B_{\mathbf{A}''})\Lambda_{\mathbf{A}''}(\phi).
\end{aligned} \tag{30}$$

By going through all combinations for $\mathbf{A}, \mathbf{A}' \in \mathcal{A}_s, \mathcal{A}_e, \mathcal{A}_v$ and using (26)–(28) as well as the condition (29), it follows that the set $\{\Lambda_{\mathbf{A}}\}_{\mathbf{A}\in\mathcal{A}}$ as defined in (30) fulfills (23). □

5.3. Definition of a basis and corresponding dual basis for a simplified configuration

In Section 5.2, we have generalized the dual compatibility condition in order to ensure the existence of a dual basis to a basis of a manifold spline space, in a general setting. In this section we discuss a simplified configuration which allows for exactly one extraordinary function in every unstructured vertex chart. For this specific example, we give an explicit construction of the dual basis. Moreover, taking advantage of the specific case considered here, we obtain dual functionals whose support is the same as the support of the corresponding functions.

In this simplified configuration we restrict ourselves to unstructured vertex charts where each segment corresponds to an element of the mesh, and give an explicit representation for the extraordinary vertex functions. Precisely, for each unstructured vertex chart ω_i, we assume that the mesh τ_i is the union of the meshes $\sigma_{i,\ell}$ on the segments $s_{i,\ell}$, where each $\sigma_{i,\ell}$ contains a single element $q_{i,\ell}$ which covers the whole segment, and assume that there exists exactly one unstructured vertex function $B_{\mathbf{A}} \in \mathcal{B}_i$. The extraordinary vertex function is continuous, has the value 1 at the extraordinary vertex, and for each element $q_{i,\ell} \in \tau_i$ there exists a d-linear mapping $\hat{\psi}_{i,\ell} : q_{i,\ell} \to]0,1[^d$, such that

$$B_{\mathbf{A}} \circ \pi_i(\boldsymbol{\zeta}) = \hat{b}_d \circ \hat{\psi}_{i,\ell}(\boldsymbol{\zeta}), \text{ for all } \boldsymbol{\zeta} \in q_{i,\ell}, \tag{31}$$

where $\hat{b}_d$ is defined as in

$$\begin{aligned}
\hat{b}_d(\zeta_1, \dots, \zeta_d) &= (1-\zeta_1)^p \dots (1-\zeta_d)^p, \\
&= b[\Xi_0](\zeta_1) \dots b[\Xi_0](\zeta_d), \quad \forall (\zeta_1, \dots, \zeta_d) \in]0,1[^d,
\end{aligned} \tag{32}$$

with $\Xi_0 = [0, \dots, 0, 1]$.

For each unstructured edge chart $\omega_i = \mathring{\omega}_i \times \bar{\omega}_i$, the mesh of the underlying bivariate chart $\mathring{\omega}_i$ is again given such that each segment $\mathring{s}_{i,\ell}$ of the bivariate chart is covered by a single element $\mathring{q}_{i,\ell}$, the one-dimensional structured chart $\bar{\omega}_i$ is partitioned into a mesh $\bar{\tau}_i = \{\bar{q}_1, \dots, \bar{q}_{m_i}\}$, and the mesh τ_i on ω_i is given via

$$\tau_i = \{\mathring{q}_{i,\ell} \times \bar{q}_k : \mathring{q}_{i,\ell} \in \mathring{\tau}_i, \bar{q}_k \in \bar{\tau}_i\}.$$

Moreover, we assume that for all $\mathbf{A}', \mathbf{A}'' \in \mathcal{A}_i$ the unstructured edge functions $B_{\mathbf{A}'}, B_{\mathbf{A}''}$ are given as in (18), where $\beta_{\mathbf{A}',i} = \beta_{\mathbf{A}'',i}$ are equal to the same unstructured vertex function of dimension $d = 2$. Hence, for each segment $\mathring{q}_{i,\ell} \times]a_{i,3}, b_{i,3}[$ there exists a bilinear mapping $\mathring{\psi}_{i,\ell} : \mathring{q}_{i,\ell} \to]0,1[^2$, such that

$$B_{\mathbf{A}} \circ \pi_i(\boldsymbol{\zeta}) = \left(\hat{b}_2 \circ \mathring{\psi}_{i,\ell}(\zeta_1, \zeta_2)\right) b[\Xi_{\mathbf{A},i,3}](\zeta_3), \qquad \text{for all } \boldsymbol{\zeta} \in \mathring{q}_{i,\ell} \times]a_{i,3}, b_{i,3}[,$$

corresponding to the representation in (18).

Given an unstructured vertex chart ω_i this means that, denoting by $j(q)$ a chart index such that $\omega_{j(q)}$ is a structured chart and $q \subset \omega_{i,j(q)}$, there exist knot vectors $\Xi_{\mathbf{A},q,j(q),1}, \dots, \Xi_{\mathbf{A},q,j(q),d}$ of the kind

$$[\underbrace{\xi', \dots, \xi'}_{p+1 \text{ times}}, \xi''] \text{ or } [\xi', \underbrace{\xi'', \dots, \xi''}_{p+1 \text{ times}}] \tag{33}$$

such that

$$B_{\mathbf{A}} \circ \pi_j(\boldsymbol{\zeta}) = b[\Xi_{\mathbf{A},q,j(q),1}](\zeta_1) \cdot \dots \cdot b[\Xi_{\mathbf{A},q,j(q),d}](\zeta_d),$$

for all $\boldsymbol{\zeta}$ such that $\psi_{j(q),i}(\boldsymbol{\zeta}) \in q$. We can now define a dual basis explicitly, using this representation. A similar representation can be derived for unstructured edge charts.

For each $\mathbf{A} \in \mathcal{A}_s$, the dual functional $\Lambda_{\mathbf{A}}$ is given as the tensor-product of univariate functionals (22). For $\mathbf{A} \in \mathcal{A}_v$, we construct the dual functional $\Lambda_{\mathbf{A}}$ by adding the contributions of each segment of the unstructured vertex chart, each being a structured subdomain. For $\mathbf{A} \in \mathcal{A}_e$, we construct the dual functional $\Lambda_{\mathbf{A}}$ analogously to the basis function in (18), that is, the tensor-product of the dual functional of a bivariate unstructured vertex function with the dual functional of a univariate B-spline in the third direction.

Theorem 3. *Given a dual-compatible spline manifold space let*

$$\mathcal{B}^* = \{\Lambda_{\mathbf{A}}, \mathbf{A} \in \mathcal{A}\}$$

be a set of functionals $\Lambda_{\mathbf{A}} : L^2(\Omega) \to \mathbb{R}$ such that:

- *for all $\mathbf{A} \in \mathcal{A}_i \cap \mathcal{A}_s$, we have*

$$\Lambda_{\mathbf{A}}(\phi) = (\lambda[\Xi_{\mathbf{A},i,1}] \otimes \dots \otimes \lambda[\Xi_{\mathbf{A},i,d}])(\phi|_{\Omega_i} \circ \pi_i), \qquad \forall \phi \in L^2(\Omega), \tag{34}$$

  where the knot vectors $\Xi_{\mathbf{A},i,k}$ are given as in (17);
- *for $\mathbf{A} \in \mathcal{A}_i \cap \mathcal{A}_v$, is the corresponding unstructured vertex function, then let $Q_{i,\ell} = \pi_i(q_{i,\ell})$ and*

$$\Lambda_{\mathbf{A}}(\phi) = \frac{1}{k_i} \sum_{\ell=1}^{k_i} \Lambda_{\mathbf{A},i,\ell}(\phi|_{Q_{i,\ell}}), \quad \forall \phi \in L^2(\Omega), \tag{35}$$

  where

$$\Lambda_{\mathbf{A},i,\ell}(\phi) = (\lambda[\Xi_0] \otimes \dots \otimes \lambda[\Xi_0])(\phi \circ \pi_i \circ (\hat{\psi}_{i,\ell})^{-1}),$$

  for all $\phi \in L^2(Q_{i,\ell})$, with $\Xi_0 = [0, \dots, 0, 1]$; and
- *for $\mathbf{A} \in \mathcal{A}_i \cap \mathcal{A}_e$, let $Q_{i,\ell} = \pi_i(\mathring{q}_{i,\ell} \times]a_{i,3}, b_{i,3}[)$, and*

$$\Lambda_{\mathbf{A}}(\phi) = \frac{1}{k_i} \sum_{\ell=1}^{k_i} \Lambda_{\mathbf{A},i,\ell}(\phi|_{Q_{i,\ell}}), \quad \forall \phi \in L^2(\Omega), \tag{36}$$

  where

$$\Lambda_{\mathbf{A},i,\ell}(\phi) = (\lambda[\Xi_0] \otimes \lambda[\Xi_0] \otimes \lambda[\Xi_{\mathbf{A},i,3}])(\phi \circ \pi_i \circ ((\mathring{\psi}_{i,\ell})^{-1}, \zeta_3)),$$

  for all $\phi \in L^2(Q_{i,\ell})$.

The set $\mathcal{B}^*$ is dual to $\mathcal{B}$, that is

$$\Lambda_{\mathbf{A}}(B_{\mathbf{A}'}) = \delta_{\mathbf{A}\mathbf{A}'}, \quad \forall \mathbf{A}, \mathbf{A}' \in \mathcal{A}.$$

Proof. It is easy to see that the $\Lambda_{\mathbf{A}}$ fulfill Definition 21, that is, the associated proto-dual functionals associated to (34)–(36) are a dual basis (in each chart). Then, it is enough to show that

$$\Lambda_{\mathbf{A}_i}(B_{\mathbf{A}_i'}) = \delta_{\mathbf{A}_i\mathbf{A}_i'}, \ \forall \mathbf{A}_i \in \mathcal{A}_i, \text{ and } \forall \mathbf{A}_i' \in \tilde{\mathcal{A}}_i. \tag{37}$$

From the dual compatibility condition, it follows that (37) is fulfilled for all $\mathbf{A} \in \mathcal{A}_i$ and $\mathbf{A}' \in \mathcal{A}$, where ω_i is a structured chart. For unstructured charts ω_i, it is obvious that

$$\Lambda_{\mathbf{A}_i}(B_{\mathbf{A}_i'}) = \delta_{\mathbf{A}_i\mathbf{A}_i'}, \ \forall \mathbf{A}_i \in \mathcal{A}_i, \text{ and } \forall \mathbf{A}_i' \in \mathcal{A}_i \cup (\mathcal{A} \setminus \tilde{\mathcal{A}}_i).$$

What remains to be shown is that $\Lambda_{\mathbf{A}_i}(B_{\mathbf{A}_i'}) = 0$ for all $\mathbf{A}_i' \in \tilde{\mathcal{A}}_i \setminus \mathcal{A}_i$. This becomes clear, as for all unstructured functions $B_{\mathbf{A}}$ the functional $\Lambda_{\mathbf{A}}$ evaluates to zero for all piecewise polynomials that are zero at the extraordinary features. This concludes the proof. □

For simplicity, we considered only one C^0 continuous extraordinary vertex function for each unstructured vertex chart. Note that one may also define a collection of extraordinary vertex functions that are discontinuous at all or some of the element boundaries within the unstructured vertex chart.

5.4. Approximation properties of spline manifolds on uniform meshes

In the following we show approximation properties for a simplified configuration. The result is based on the construction of a stable dual basis, from which one can define a projection operator and use it to prove approximation properties of the spline manifold space. In this section we consider uniform, regular meshes as in Lemma 4. Note that the results can be extended easily to more general configurations, by suitably extending the scope of Lemma 4.

Here we consider h-refinement: a spline manifold Ω is given, with an initial mesh $\mathcal{T}_{h_0}$ over it. From this we construct a family of meshes $\{\mathcal{T}_h\}$ by mesh refining each structured chart. The refinement has to be consistent with the manifold structure, fulfilling Definition 3, in particular (3), and Definitions 7–9. Note that during h-refinement the structured charts and transition functions between them are unchanged, while we modify the unstructured charts in such a way that only the elements adjacent to an extraordinary vertex are included in those charts. Accordingly, we assume that a family of nested spaces $\{\mathcal{S}_h\}$ is given. The subscript h always denotes the dependence on the refinement level.

A spline manifold domain Σ is given by a coarse mesh parametrization $\mathbf{G} \in (\mathcal{S}_{h_0})^3$, as in (19). For simplicity, we consider a bivariate Ω, then Σ is a closed surface in the space $\mathbb{R}^3$. During h-refinement $\mathbf{G}$ is kept unchanged. This gives a sequence of nested isogeometric spaces $\mathcal{V}_h$ via (20).

To study the approximation properties of $\mathcal{V}_h$ we follow the approach in, e.g., Bazilevs et al. (2006), Beirão da Veiga et al., (2012b, 2013) for structured spline spaces, which applies to the present framework as well. To keep it simple, we focus on a simple configuration: we consider a manifold obtained by merging tensor-product patches with C^{p-1} continuity except around the extraordinary vertices, where the continuity is only C^0. This configuration is referred to as *multi-patch B-splines with enhanced smoothness* as in Buchegger et al. (2015), where it has been first introduced and studied in the context of IgA. On the coarsest mesh $\mathcal{T}_{h_0}$, the length of the C^0 lines is $p+1$ element edges, which corresponds to the condition that a function in $\mathcal{S}_{h_0}$ is C^0 across the patch interfaces if and only if it has an extraordinary vertex in the closure of its support. The structured charts for this configuration can be taken as the union of each pair of patches that have a common interface. For each unstructured vertex there exists an unstructured vertex chart composed of all elements in the one-ring around, i.e. all elements that contain the unstructured vertex in their closure. This is not the only possibility but it simplifies the next steps. In this case each transition function $\psi_{i,j}$ between structured charts is the composition of a translation and a rotation by a multiple of $\frac{\pi}{2}$. To further simplify, we assume the mesh on each structured chart is uniform with mesh-size h.

We assume by construction that each space $\mathcal{S}_h$ is *complete*. By this, we mean that for every structured chart ω_i the set $\tilde{\mathcal{B}}_i$ spans all piecewise polynomials of degree p and continuity stated above.

The space $L^2(\Omega)$ is defined as

$$L^2(\Omega) = \left\{ \phi : \Omega \to \mathbb{R} \mid \phi \circ \pi_i \in L^2(\omega_i) \ \text{ for all structured charts } \omega_i \right\},$$

having the corresponding norm

$$\|\phi\|^2_{L^2(\Omega)} = \sum_{Q \in \mathcal{T}_h} \|\phi \circ \pi_{i,Q}\|^2_{L^2(\pi^{-1}_{i,Q}(Q))}, \tag{38}$$

where $\omega_{i,Q}$ is a structured chart covering Q, i.e. $Q \subseteq \pi_{i,Q}(\omega_{i,Q})$. Due to the isometry of the transition function, the L^2-norm of a function defined on a chart fulfills $\|\varphi\|^2_{L^2(\omega_{i,j})} = \|\varphi \circ \psi_{j,i}\|^2_{L^2(\omega_{j,i})}$ for all structured charts ω_i, ω_j. Hence, the L^2-norm on Ω is well-defined because all elements are covered by structured charts. Moreover, the definition of the L^2-norm is independent of the level of refinement. We define bent Sobolev spaces $\mathcal{H}^k(\Omega)$ in the same fashion. Bent Sobolev spaces are piecewise Sobolev spaces with some regularity at the element interfaces, see Bazilevs et al. (2006), Beirão da Veiga et al. (2014). For example, the space $\mathcal{H}^{p+1}(\Omega)$ is defined as the closure of the space of piecewise C^∞ functions having the same continuity at the mesh lines of the space $\mathcal{S}_{h_0}$, with respect to the norm

$$\|\phi\|^2_{\mathcal{H}^{p+1}(\Omega)} = \|\phi\|^2_{L^2(\Omega)} + \sum_{k=1}^{p+1} |\phi|^2_{\mathcal{H}^k(\Omega)}, \tag{39}$$

where

$$|\phi|^2_{\mathcal{H}^k(\Omega)} = \sum_{Q \in \mathcal{T}_h} |\phi \circ \pi_{i,Q}|^2_{H^k(\pi^{-1}_{i,Q}(Q))} \tag{40}$$

and $|\cdot|_{H^k(q)}$ is the usual k-th order Sobolev seminorm. Obviously, all the spaces and norms can be defined accordingly on subdomains of Ω and are independent of the level of refinement.

Using the dual basis defined in Theorem 3 we introduce a projection operator $\Pi_{\mathcal{S}_h} : L^2(\Omega) \to \mathcal{S}_h$ onto the B-spline manifold space via

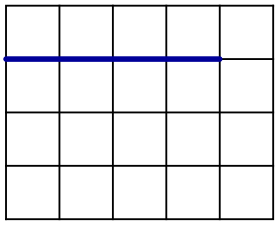

Fig. 6. Possible configuration of a box R and mesh line $\mathbf{e}$ for degree $p = 2$. (For interpretation of the references to color in this figure, the reader is referred to the web version of this article.)

$$\phi \mapsto \Pi_{\mathcal{S}_h}(\phi) = \sum_{\mathbf{A} \in \mathcal{A}_h} \Lambda_{\mathbf{A}}(\phi) B_{\mathbf{A}} \tag{41}$$

The projector is L^2 stable, uniformly with respect to h, i.e.

$$\|\phi - \Pi_{\mathcal{S}_h}(\phi)\|_{L^2(\Omega)} \leq C \|\phi\|^2_{L^2(\Omega)}, \qquad \forall \phi \in L^2(\Omega), \tag{42}$$

which follows directly from the L^2 stability of the dual basis as defined in Theorem 3, see for example Beirão da Veiga et al. (2014). To prove its approximation properties we use the following Lemma.

Lemma 4. *Let $\mathcal{S}_R$ be the space of all piecewise polynomials with respect to a uniform Cartesian mesh of a box $R \in \mathbb{R}^2$, such that*

- *the mesh is formed by up to $2p+1$ elements per direction with meshsize h;*
- *the polynomial degree is p in each direction; and*
- *the continuity is C^{p-1} globally with the exception of a mesh line $\mathbf{e}$ where the continuity is only C^0, i.e., $\mathcal{S}_R \subset C^{p-1}(R \setminus \mathbf{e}) \cap C^0(R)$.*

Let $\mathcal{H}^{p+1}(R)$ be the bent Sobolev space associated to $\mathcal{S}_R$. Then for all $\phi \in \mathcal{H}^{p+1}(R)$ there exists a $\rho \in \mathcal{S}_R$ such that

$$\|\phi - \rho\|_{L^2(R)} \leq C h^{p+1} |\phi|_{\mathcal{H}^{p+1}(R)} \tag{43}$$

with a constant C only dependent on p.

Proof. The size of R depends on the number of elements $\mathbf{n} = (n_1, n_2)$ in each direction and the element size h. Given $\phi \in \mathcal{H}^{p+1}(R)$ there exists indeed $\rho \in \mathcal{S}_R$ such that

$$\|\phi - \rho\|_{L^2(R)} \leq C(p, h, \mathbf{n}, \mathbf{e}) |\phi|_{\mathcal{H}^{p+1}(R)}$$

with $C(p, h, \mathbf{n}, \mathbf{e})$ independent of ϕ. The proof is the same as for the classical Bramble–Hilbert lemma, see, e.g., Bazilevs et al. (2006). The dependence of the constant with respect to h, that is $C(p, h, \mathbf{n}, \mathbf{e}) = C(p, \mathbf{n}, \mathbf{e}) h^{p+1}$, follows from a scaling argument. Finally, there are a finite number of different configurations for $\mathbf{n}$ and $\mathbf{e}$, therefore we can set $C(p) = \max_{\mathbf{n}, \mathbf{e}} C(p, \mathbf{n}, \mathbf{e})$. □

See Fig. 6 for a possible configuration of R. Here, the line of C^0 continuity is shown in blue.

Given $Q \in \mathcal{T}_h$, we define $\widetilde{Q} \subset \Omega$ in the following way: for each structured chart ω_i, $\widetilde{Q} \cap \Omega_i$ is the minimal box containing all the supports of functions in $\mathcal{B}_h$ whose support contains Q. We can now state the local approximation estimate.

Theorem 5. *Under the assumptions of this Section, for $\phi \in \mathcal{H}^{p+1}(\widetilde{Q})$ it holds*

$$\|\phi - \Pi_{\mathcal{S}_h}(\phi)\|_{L^2(Q)} \leq C h^{p+1} |\phi|_{\mathcal{H}^{p+1}(\widetilde{Q})}, \tag{44}$$

where the constant C depends only on p.

Proof. The first step of the proof is to show that, given $\phi \in \mathcal{H}^{p+1}(\widetilde{Q})$, there exists $\rho \in \mathcal{S}_h$ such that

$$\|\phi - \rho\|_{L^2(\widetilde{Q})} \leq C h^{p+1} |\phi|_{\mathcal{H}^{p+1}(\widetilde{Q})}. \tag{45}$$

We are in one of two cases, either

(a) $\widetilde{Q}$ contains an extraordinary vertex, or
(b) $\widetilde{Q} \subset \pi_i(\omega_i)$ where ω_i is a structured chart.

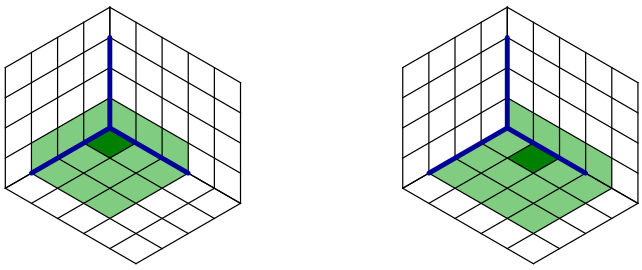

Fig. 7. Different types of support extensions $\widetilde{Q}$ for $p = 2$. (For interpretation of the references to color in this figure, the reader is referred to the web version of this article.)

See Fig. 7 for a representation of the two possible cases. In the figure the C^0-continuity lines are depicted in blue. The dark green element represents Q and the light green region represents its support extension $\widetilde{Q}$. Due to the assumption on the length of the C^0 lines, case (a) only occurs when Q is adjacent to an extraordinary vertex, i.e., there exists an unstructured chart ω_i such that $Q \subset \pi_i(\omega_i)$. In this case we can split $\widetilde{Q}$ into $\widetilde{Q}_1, \dots, \widetilde{Q}_{k_i}$ such that each $\widetilde{Q}_\ell$ intersects only the segment $\pi_i(s_{i,\ell})$ (see Definition 7). Each $\mathcal{S}_h|_{\widetilde{Q}_\ell}$ is a standard tensor-product spline space therefore we can use (Beirão da Veiga et al., 2014, Section 2.2.2 and Section 4.4) in order to construct splines $\rho_\ell \in \mathcal{S}_h|_{\widetilde{Q}_\ell}$ which approximate $\phi|_{\widetilde{Q}_\ell}$ and match continuously in the whole $\widetilde{Q}$. Since on the coarsest mesh the C^0 lines at the extraordinary vertex cover $p+1$ element edges (see Fig. 7), each interface between two adjacent sets of $\widetilde{Q}_1, \dots, \widetilde{Q}_{k_i}$ is covered by the C^0 continuity lines of $\rho \in \mathcal{S}_h$ and (45) follows. In case (b), we can use Lemma 4, then (45) follows by (43).

Having (45) and recalling the L^2 stability of the projector $\Pi_{\mathcal{S}_h}$, (44) is derived in the usual way, i.e.

$$\begin{aligned}\|\phi - \Pi_{\mathcal{S}_h}(\phi)\|_{L^2(Q)} &= \|\phi - \rho - \Pi_{\mathcal{S}_h}(\phi - \rho)\|_{L^2(Q)} \\ &\le C\|\phi - \rho\|_{L^2(\widetilde{Q})} \\ &\le Ch^{p+1}|\phi|_{\mathcal{H}^{p+1}(\widetilde{Q})}.\end{aligned}$$

The stability constant as well as the approximation constant only depend on p, which concludes the proof. □

By means of inverse estimates and generalizing (45), (44) can be extended to higher order Sobolev norms. For $0 \le q \le p+1$ it holds

$$|\phi - \Pi_{\mathcal{S}_h}(\phi)|_{H^q(Q)} \le Ch^{p-q+1}|\phi|_{\mathcal{H}^{p+1}(\widetilde{Q})}, \tag{46}$$

where the constant C depends only on p and q. The details are not reported for the sake of brevity.

We can extend the result to the spline manifold domain Σ, in this case a closed surface in $\mathbb{R}^3$, parametrized by $\mathbf{G} \in (\mathcal{S}_{h_0})^3$. We assume that $\mathbf{G}$ is regular, that is, there exist constants $\underline{c}, \overline{c}$, with

$$\overline{c} \ge \det(\nabla\mathbf{G}^T(\mathbf{x})\nabla\mathbf{G}(\mathbf{x})) \ge \underline{c} > 0$$

for all $\mathbf{x} \in Q$ and for all $Q \in \mathcal{T}_{h_0}$. Note that, in general, we cannot define Sobolev spaces of any order on Σ, due to the lack of smoothness of the manifold itself. However the L^2 space on Σ can be defined as

$$L^2(\Sigma) = \{f : f \circ \mathbf{G} \in L^2(\Omega)\}$$

and the corresponding norm is given via

$$\|f\|_{L^2(\Sigma)} = \|f \circ \mathbf{G}\,(\det(\nabla\mathbf{G}^T\nabla\mathbf{G}))^{1/4}\|_{L^2(\Omega)}.$$

The bent Sobolev spaces can be defined similarly, as in (39)–(40). See Hebey (1996, 2000) for more details about Sobolev spaces on manifolds. Then, for all $f \in L^2(\Sigma)$, we can define the isogeometric projector

$$\Pi_{\mathcal{V}_h}(f) = \Pi_{\mathcal{S}_h}(f \circ \mathbf{G}) \circ \mathbf{G}^{-1}.$$

Approximation properties of $\Pi_{\mathcal{V}_h}$ easily follow from the ones of $\Pi_{\mathcal{S}_h}$ stated in Theorem 5, following the same approach as in Bazilevs et al. (2006), Dedè and Quarteroni (2015).

Theorem 6. *Under the assumptions of this Section, for all* $f \in \mathcal{H}^{p+1}(\Sigma)$

$$\|f - \Pi_{\mathcal{V}_h}(f)\|_{L^2(\Sigma)} \le Ch^{p+1}\|f\|_{\mathcal{H}^{p+1}(\Sigma)}, \tag{47}$$

where the constant C depends only on $\mathbf{G}$ and p.

Note that all the results presented here extend naturally to volumetric domains. In that case, the lines of C^0 continuity extend to faces of C^0 continuity in a vicinity of the extraordinary vertices and edges. In this case it is necessary that the spaces obtained after each refinement step are dual-compatible

Remark 6. The same ideas can be applied to extend the convergence results to T-spline manifolds, assuming again that the continuity across patches is C^0 in the vicinity of the extraordinary vertices, and this continuity is preserved when refining. Assuming that the coarsest spline space is a T-spline space, bent Sobolev spaces can be defined according to the T-spline characterization in Bressan et al. (2015). It is also necessary that the spaces obtained during refinement are nested and dual-compatible, which can be accomplished with the refinement of Morgenstern and Peterseim (2015). We prefer not to present the T-spline case here, to avoid explaining all the technical details.

6. Conclusion and possible extensions

We have introduced a general mathematical framework, based on manifolds, for the definition and the analysis of unstructured spline spaces. As it is done in Grimm and Hughes (1995) the main idea is to decompose the domain into charts, which are meshed with quadrilaterals or hexahedra. Then spline basis functions and dual functionals can be defined locally on each chart. Unstructured charts are necessary to cover extraordinary vertices and edges of the domain.

We have used this framework to generalize the dual-compatibility condition of Beirão da Veiga et al. (2012a, 2013) to unstructured spline spaces, and in particular to analyze the approximation properties of splines with high continuity everywhere except in the vicinity of extraordinary vertices and edges, where the continuity is only C^0. Although the analysis was restricted to the low continuity case, the framework allows for the definition of spline functions with higher smoothness, and their analysis will be the aim of future work.

In our definitions the physical domain is necessarily a manifold. However, since we are defining the charts in the parametric domain, and not in the physical domain, it is possible to extend our framework to non-manifold domains using special bifurcation charts (such as T-shaped or X-shaped charts for curves, etc.) This could be of interest for certain beam or shell formulations, or for the proper representation of the medial axis or medial surface of an object, for instance.

Finally, for the sake of simplicity we have restricted ourselves to B-splines and T-splines on quadrilateral/hexahedral meshes. The framework can be generalized to other spline spaces, such as NURBS or trigonometric splines.

Acknowledgements

The authors were partially supported by the European Research Council through the FP7 ERC Consolidator Grant n.616563 *HIGEOM*, and by the Italian MIUR through the PRIN "Metodologie innovative nella modellistica differenziale numerica". This support is gratefully acknowledged.

Appendix A. Spline manifolds with boundary

We can extend the definition of a spline manifold to a manifold with boundary. To do so, we first need to extend Definition 1, defining a suitable proto-manifold that takes into account the boundary.

Definition 23 *(Proto-manifold with boundary).* A *proto-manifold with boundary* is a generalization of a proto-manifold, where the charts $\{\omega_i\}_{i=1,\dots,N}$ are given as $\omega_i = \mathit{interior}\,(\omega_i) \cup \gamma_i$, such that $\mathit{interior}\,(\omega_i)$ are open polytopes forming a standard proto-manifold (with transition domains $\mathit{interior}\,(\omega_{i,j})$ and transition functions $\psi_{i,j}$) and each $\gamma_i \subset \partial\omega_i$ is a part of the boundary of the chart $\mathit{interior}\,(\omega_i)$. Moreover, the transition domains fulfill $\omega_{i,j} = \mathit{interior}\,(\omega_{i,j}) \cup \gamma_{i,j}$, with $\gamma_{i,j} = \gamma_i \cap \partial\omega_{i,j}$, and the transition functions are the continuous extensions of $\psi_{i,j}$ and map $\gamma_{i,j}$ onto $\gamma_{j,i}$ and $\mathit{interior}\,(\omega_{i,j})$ onto $\mathit{interior}\,(\omega_{j,i})$.

Similar to the standard parameter manifold in Definition 2, we can define the *parameter manifold with boundary* Ω via the equivalence relation induced by the transition functions. Since the transition functions always map the interior onto the interior and the boundary onto the boundary, the parameter manifold Ω can be separated into $\mathit{interior}\,(\Omega)$ and the boundary denoted by Γ.

This definition of the boundary of the (open) parameter manifold is equivalent to the classical definition of a manifold with boundary, as discussed in Grimm and Hughes (1995). In this case every boundary point of the manifold has a neighborhood that is homeomorphic to the *half d-ball*. Note that the boundary Γ itself can be interpreted as a topological manifold of dimension $d-1$.

For the definition of the spline spaces, we assume the following.

Assumption 24. The local boundary γ_i is conforming with respect to the elements, i.e. there exists a subset of faces of elements $q \in \tau_i$ that forms a mesh for the boundary γ_i.

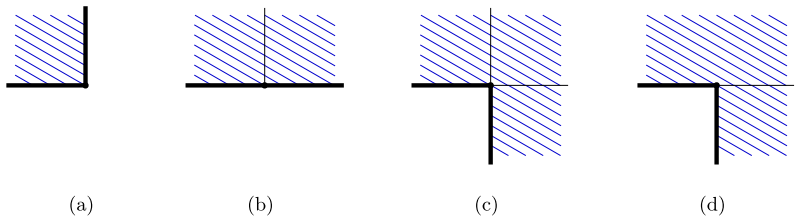

Fig. A.8. Different types of valid (a)–(c) and non-valid (d) boundary vertices in 2D.

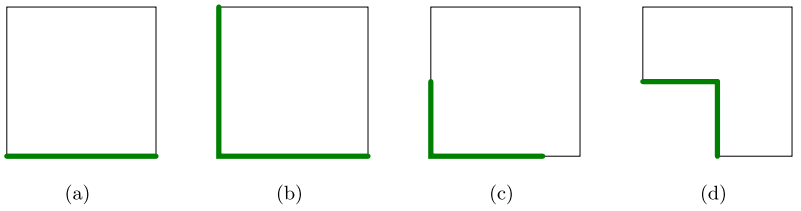

Fig. A.9. Structured charts with boundary (a)–(c) and boundary chart (d) in 2D.

Table A.3
Classification of valid boundary edges and vertices in 3D.

Structured edge	Regular boundary edge
Structured vertex	Regular boundary vertex
	Hanging boundary vertex
Unstructured vertex	Partially unstructured boundary vertex

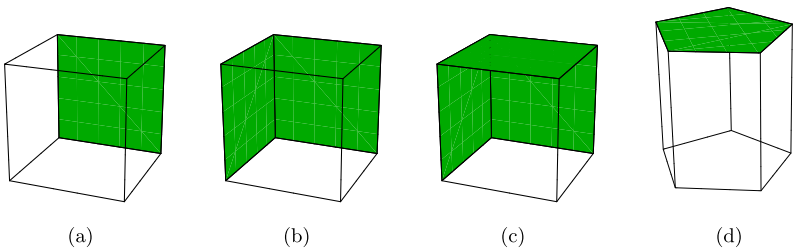

Fig. A.10. Structured charts with boundary (a)–(c) and unstructured edge chart with boundary (d) in 3D.

To be able to define manifolds with boundary containing non-convex features, we need additional types of charts, so called boundary charts. To avoid the tedious formal definition of boundary charts, we present figures that should explain the ideas behind. In Fig. A.8 we present different types of two-dimensional boundary vertices, regular boundary vertices (a)–(c), as well as a non-regular boundary vertex (d). The vertices in Figs. A.8(a) and A.8(b) can be covered by the boundaries of structured charts (see Fig. A.9(a)–A.9(c)). For the vertex in Fig. A.8(c) we need a special boundary chart (see Fig. A.9(d)), associated with the function which is non-zero at the corner. Note that the boundary vertex in Fig. A.8(d) is discarded since it does not allow for functions that are non-zero at the corner.

In the three-dimensional case, there are more different configurations to consider, which are listed in Table A.3. Here, we need to consider two different types of boundary charts.

Figs. A.10 and A.11 depict several possible three-dimensional charts with boundary. In Figs. A.10(a)–A.10(c) we show several examples of structured charts with boundary. Fig. A.10(d) shows an unstructured edge chart with boundary. In Fig. A.11 we show the two different types of unstructured boundary charts that are needed to represent all meshes of practical interest. The one in Fig. A.11(a) is the Cartesian product of a two-dimensional boundary chart with an interval in the third direction. The chart depicted in Fig. A.11(b) is a boundary chart corresponding to a non-convex vertex at the boundary. One can include more complex boundary configurations by introducing unstructured boundary charts, which we will not consider for the sake of simplicity.

Concerning spline manifold spaces on parameter manifolds with boundary, we need to adjust the condition on proto-basis functions in equation (6) to the following one

$$\lim_{\boldsymbol{\zeta}\to\partial\omega_i\setminus\gamma_i} b_{\mathbf{A}_i}(\boldsymbol{\zeta}) = 0. \tag{A.1}$$

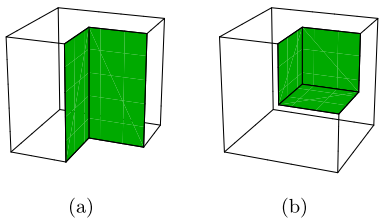

Fig. A.11. Boundary charts in 3D.

With this modification, the spline manifold space can interpolate at the boundary. The theory concerning dual-compatibility and approximation properties presented in Section 5 can be generalized directly to spline manifolds with boundary. Most importantly, both Theorems 5 and 6 extend directly to manifolds with boundary, using the boundary charts introduced here. Thus extending the approximation error bounds to manifolds with boundary of general topology.

References

Barendrecht, P.J., Shen, J., Kosinka, J., Sabin, M., Dodgson, N., 2013. Isogeometric Analysis with Subdivision Surfaces. Eindhoven University of Technology, Eindhoven, the Netherlands.

Bazilevs, Y., Beirão da Veiga, L., Cottrell, J., Hughes, T., Sangalli, G., 2006. Isogeometric analysis: approximation, stability and error estimates for h-refined meshes. Math. Models Methods Appl. Sci. 16 (07), 1031–1090.

Beirão da Veiga, L., Buffa, A., Cho, D., Sangalli, G., 2011. Isogeometric analysis using T-splines on two-patch geometries. Comput. Methods Appl. Mech. Eng. 200 (21–22), 1787–1803.

Beirão da Veiga, L., Buffa, A., Cho, D., Sangalli, G., 2012a. Analysis-suitable T-splines are dual-compatible. Comput. Methods Appl. Mech. Eng. 249, 42–51.

Beirão da Veiga, L., Cho, D., Sangalli, G., 2012b. Anisotropic NURBS approximation in isogeometric analysis. Comput. Methods Appl. Mech. Eng. 209, 1–11.

Beirão da Veiga, L., Buffa, A., Sangalli, G., Vázquez, R., 2013. Analysis-suitable T-splines of arbitrary degree: definition, linear independence and approximation properties. Math. Models Methods Appl. Sci. 23 (11), 1979–2003.

Beirão da Veiga, L., Buffa, A., Sangalli, G., Vázquez, R., 2014. Mathematical analysis of variational isogeometric methods. Acta Numer. 23, 157.

Bressan, A., Buffa, A., Sangalli, G., 2015. Characterization of analysis-suitable T-splines. Comput. Aided Geom. Des. 39, 17–49.

Buchegger, F., Jüttler, B., Mantzaflaris, A., 2015. Adaptively refined multi-patch B-splines with enhanced smoothness. Appl. Math. Comput. In press.

Burkhart, D., Hamann, B., Umlauf, G., 2010. Iso-geometric finite element analysis based on Catmull–Clark: subdivision solids. Comput. Graph. Forum 29 (5), 1575–1584. http://dx.doi.org/10.1111/j.1467-8659.2010.01766.x.

Catmull, E., Clark, J., 1978. Recursively generated B-spline surfaces on arbitrary topological meshes. Comput. Aided Des. 10 (6), 350–355.

Cirak, F., Ortiz, M., 2001. Fully C1-conforming subdivision elements for finite deformation thin-shell analysis. Int. J. Numer. Methods Eng. 51 (7), 813–833.

Cirak, F., Ortiz, M., Schroder, P., 2000. Subdivision surfaces: a new paradigm for thin-shell finite-element analysis. Int. J. Numer. Methods Eng. 47 (12), 2039–2072.

Collin, A., Sangalli, G., Takacs, T., 2015. Analysis-suitable G^1 multi-patch parametrizations for C^1 isogeometric spaces. Preprint, arXiv:1509.07619.

Cottrell, J.A., Hughes, T.J.R., Bazilevs, Y., 2009. Isogeometric Analysis: Toward Integration of CAD and FEA. John Wiley & Sons.

Dedè, L., Quarteroni, A., 2015. Isogeometric analysis for second order partial differential equations on surfaces. Comput. Methods Appl. Mech. Eng. 284, 807–834.

Dokken, T., Lyche, T., Pettersen, K.F., 2013. Polynomial splines over locally refined box-partitions. Comput. Aided Geom. Des. 30 (3), 331–356.

Doo, D., Sabin, M., 1978. Behaviour of recursive division surfaces near extraordinary points. Comput. Aided Des. 10 (6), 356–360.

Grimm, C.M., Hughes, J.F., 1995. Modeling surfaces of arbitrary topology using manifolds. In: Proceedings of the 22nd Annual Conference on Computer Graphics and Interactive Techniques. ACM, pp. 359–368.

Groisser, D., Peters, J., 2015. Matched G^k-constructions always yield C^k-continuous isogeometric elements. Comput. Aided Geom. Des. 34, 67–72.

Hebey, E., 1996. Sobolev Spaces on Riemannian Manifolds, vol. 1635. Springer Science & Business Media.

Hebey, E., 2000. Nonlinear Analysis on Manifolds: Sobolev Spaces and Inequalities, vol. 5. American Mathematical Soc.

Hughes, T.J.R., Cottrell, J.A., Bazilevs, Y., 2005. Isogeometric analysis: CAD, finite elements, NURBS, exact geometry and mesh refinement. Comput. Methods Appl. Mech. Eng. 194 (39–41), 4135–4195.

Jüttler, B., Kapl, M., Nguyen, D.-M., Pan, Q., Pauley, M., 2014. Isogeometric segmentation: the case of contractible solids without non-convex edges. Comput. Aided Des. 57 (0), 74–90.

Jüttler, B., Mantzaflaris, A., Perl, R., Rumpf, M., 2015. On isogeometric subdivision methods for PDEs on surfaces. arXiv preprint, arXiv:1503.03730.

Kapl, M., Buchegger, F., Bercovier, M., Jüttler, B., 2015a. Isogeometric analysis with geometrically continuous functions on multi-patch geometries. NFN technical report No. 35.

Kapl, M., Vitrih, V., Jüttler, B., Birner, K., 2015b. Isogeometric analysis with geometrically continuous functions on two-patch geometries. Comput. Math. Appl. 70 (7), 1518–1538.

Kiendl, J., Bazilevs, Y., Hsu, M.-C., Wüchner, R., Bletzinger, K.-U., 2010. The bending strip method for isogeometric analysis of Kirchhoff–Love shell structures comprised of multiple patches. Comput. Methods Appl. Mech. Eng. 199 (35), 2403–2416.

Kleiss, S.K., Pechstein, C., Jüttler, B., Tomar, S., 2012. IETI – isogeometric tearing and interconnecting. Comput. Methods Appl. Mech. Eng. 247–248, 201–215.

Lee, B.-G., Lyche, T., Mørken, K., 2001. Some examples of quasi-interpolants constructed from local spline projectors. In: Mathematical Methods for Curves and Surfaces. Oslo, 2000. In: Innov. Appl. Math.. Vanderbilt Univ. Press, Nashville, TN, pp. 243–252.

Morgenstern, P., Peterseim, D., 2015. Analysis-suitable adaptive T-mesh refinement with linear complexity. Comput. Aided Geom. Des. 34, 50–66.

Nguyen, D.-M., Pauley, M., Jüttler, B., 2014a. Isogeometric segmentation. Part II: on the segmentability of contractible solids with non-convex edges. In: Geometric Modeling and Processing 2014. Graph. Models 76 (5), 426–439.

Nguyen, T., Karčiauskas, K., Peters, J., 2014b. A comparative study of several classical, discrete differential and isogeometric methods for solving Poisson's equation on the disk. Axioms 3 (2), 280–299.

Nguyen, T., Karčiauskas, K., Peters, J., 2016. C1 finite elements on non-tensor-product 2d and 3d manifolds. Appl. Math. Comput. 272 (P1), 148–158.

Owen, S.J., 1998. A survey of unstructured mesh generation technology. In: IMR, pp. 239–267.

Rourke, C.P., Sanderson, B.J., 1972. Introduction to Piecewise-Linear Topology, Springer Study Edition. Springer, Berlin.

Schumaker, L.L., 2007. Spline Functions: Basic Theory, third edition. Cambridge Mathematical Library. Cambridge University Press, Cambridge.

Scott, M., Simpson, R., Evans, J., Lipton, S., Bordas, S., Hughes, T., Sederberg, T., 2013. Isogeometric boundary element analysis using unstructured T-splines. Comput. Methods Appl. Mech. Eng. 254 (0), 197–221.
Scott, M.A., Thomas, D.C., Evans, E.J., 2014. Isogeometric spline forests. Comput. Methods Appl. Mech. Eng. 269, 222–264.
Sederberg, T., Zheng, J., Bakenov, A., Nasri, A., 2003. T-splines and t-NURCCSs. ACM Trans. Graph. 22 (3), 477–484.
Siqueira, M., Xu, D., Gallier, J., Nonato, L.G., Morera, D.M., Velho, L., 2009. Technical section: a new construction of smooth surfaces from triangle meshes using parametric pseudo-manifolds. Comput. Graph. 33 (3), 331–340.
Wang, W., Zhang, Y., Scott, M.A., Hughes, T.J.R., 2011. Converting an unstructured quadrilateral mesh to a standard T-spline surface. Comput. Mech. 48 (4), 477–498.
Wang, W., Zhang, Y., Xu, G., Hughes, T.J.R., 2012. Converting an unstructured quadrilateral/hexahedral mesh to a rational T-spline. Comput. Mech. 50 (1), 65–84.
Xu, G., Mourrain, B., Duvigneau, R., Galligo, A., 2013. Analysis-suitable volume parameterization of multi-block computational domain in isogeometric applications. In: Solid and Physical Modeling 2012. Comput. Aided Des. 45 (2), 395–404.